Improved multi-body rope approach for free-form gridshell structures using equal-length element strategy

Improved Multi-body Rope Approach for Free-Form Gridshell Structures Using Equal-Length Element Strategy

Amedeo Manuello Bertetto[a], Jonathan Melchiorre[a,*], Giuseppe Carlo Marano[a,b]

[a] *Politecnico di Torino, DISEG, Department of Structural, Geotechnical and Building Engineering, Corso Duca Degli Abruzzi, 24, Turin, 10129, Italy*
[b] *Fuzhou University, College of Civil Engineering, Xueyuan Rd, Gulou District, Fuzhou, 350025, China*

Abstract

Gridshell roofing constructions are favoured in modern engineering and architecture for their capacity to produce expansive, lightweight roofs using slender main structural elements, yet their complex and costly fabrication limits broader adoption. The Multi-body Rope Approach (MRA) is effective in computing structurally efficient geometries in gridshells, emphasizing the need to optimize design configurations for minimal internal stresses. This paper presents two strategies, Multiple Order MRA (MO-MRA) and Repulsive Nodes MRA (RN-MRA), to improve the MRA and streamline gridshell construction by reducing the necessary types of structural components. These approaches are combined in an improved MRA (i-MRA), reducing manufacturing costs and increasing efficiency in construction management. The i-MRA was implemented in Matlab and tested on four case studies of increasing complexity, demonstrating its effectiveness.

Keywords: Form finding, Gridshell, Structural Optimization, Construction Process, Structural engineering

1. Introduction

In recent years, there has been a growing demand for architectural structures that offer greater internal distribution flexibility and allow for free-form

*Corresponding author.
Email address: jonathan.melchiorre@polito.it (Jonathan Melchiorre)

designs in big-span roofing projects. Double-curved shells and domes have emerged as a feasible alternative for achieving at the same time column-free spaces and complex shapes [1]. Free-form shell structures, also known as curved shell structures, have gained significant attention due to their unique and aesthetically pleasing qualities [2]. These structures feature complex, curved shapes that challenge traditional construction methods and require innovative design and engineering solutions.

Free-form shell structures are widely used in the construction of large-scale buildings. Shells are self-supporting thin structures with single or double curvature that can cover broad-span areas without the need for beams, columns, or walls. Their curved shape provides an ideal morphology for various load patterns and multiple stress paths, making them highly efficient. In shell constructions, membrane actions are primarily related to plane stress, while bending deformation can result in secondary forces. The most desirable behaviour for shells is the membranous one, as it exhibits higher structural efficiency. However, if compressive membrane states are present, sufficient bending stiffness must be provided to prevent local (buckling) and non-local (snap-through) instability problems.

A gridshell is a type of free-form shell structure that comprises a three-dimensional grid of linear elements interconnected by nodes. This unique structure exhibits the mechanical behaviour of shells and combines the soft curves of shell structures with the rigidity and strength of structural grids. As a result, gridshells offer a range of structural and aesthetic benefits. They are lightweight, self-supporting structures that can span large areas while minimizing material usage. Recent studies have demonstrated the potential

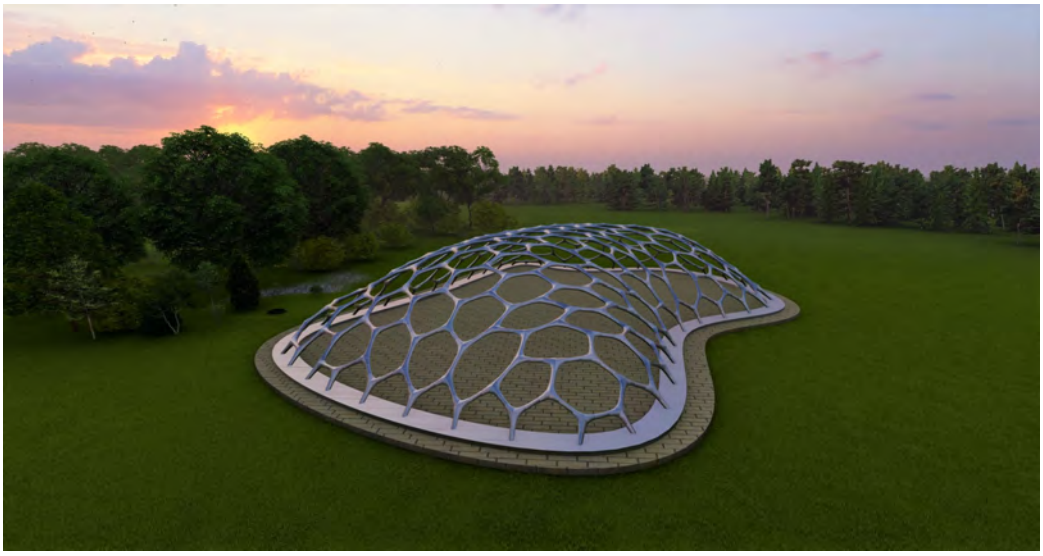

Figure 1: Free-form gridshell structure generated with Multi-body Rope Approach.

of gridshells for structural applications, including in the fields of architecture, engineering, and design [3, 4].

Gridshell structures have a rich history dating back to the mid-20th century, when architects and engineers began to experiment with innovative materials and structural systems. Among the earliest examples of gridshell design was the Zeiss Planetarium in Jena, Germany, completed in 1923, featuring a dome made of thin, curved wood panels.

In the 1960s and 70s, architects and engineers like Frei Otto [5] and Ted Happold [6, 7] pioneered new approaches to gridshell design. They used lightweight materials and computer modelling to create complex, double-curved forms. Early gridshells were commonly built with materials such as timber [8] or fabric and were used to create vast open spaces like exhibition halls, sports arenas [9], and airport terminals.

In recent decades, advances in digital design and fabrication technologies

have allowed architects and engineers to push the boundaries of gridshell design even further. Gridshell structures are now commonly made from materials such as steel [10, 11], aluminium [12], wood [13, 14, 15, 16], and elastic composite materials [17, 18, 19].

Despite their many advantages, the construction of gridshell structures remains limited due to the complexity of their geometry and structural challenges [20]. In addition, the need for expensive assembly technologies and precise form-finding to ensure stability has made the design and construction of gridshells a challenging task.

Moreover, the lack of data on this structural typology has hindered its wider adoption in the industry [21]. However, recent advancements in computing systems have greatly improved the ability to analyze increasingly complex systems, making gridshell architecture an increasingly viable option [22]. As a result, continued growth in the use of gridshells in the design and construction of large, open structures can be expected in the years to come.

Gridshell structures are defined by the interaction between their shape and stress distribution. Because of this relationship between shape and forces, designing such structures directly, as in the case of conventional structures, is ineffective. In this scenario, the search for a suitable structural shape is critical, both for design aesthetics and, more importantly, for the structure's capability to support loads. To achieve a feasible shape, it is necessary to balance the internal forces and loads acting on the structure and minimize the bending moment within the resisting elements [23]. Form-finding is a vital step in designing free-form gridshell structures, where the optimal shape and layout of the structural elements are determined under a specific load

pattern. Various form-finding methods have been developed over the years to facilitate the design of these complex structures, including both physical and computational modelling techniques [24]. Among the most popular form-finding methods are the force density method [25], thrust network analysis [26], dynamic relaxation method [27], particle-spring system [28], multi-body rope approach [29], and others [30, 31, 32].

The primary objective of these techniques is to identify a structural shape that meets the boundary requirements, reduces the cost of construction, and has an aesthetically pleasing appearance. The cutting-edge trend in structural design research involves coupling innovative shapes and free-form structures with structural optimization [33, 34, 35]. A significant challenge lies in defining a structural model that is optimized not only structurally but also geometrically and constructively. Additionally, optimizing the production of the structural elements and managing the construction stages poses a final challenge in form-finding and optimization.

To overcome these challenges, architects and engineers have developed several techniques and tools to optimize the design of structural elements, panelling patterns [36, 37], and nodes [38, 39] in gridshells. These may include digital simulations and models, advanced material analysis techniques, and the use of parametric design tools to explore and refine different design options.

This paper presents an original development for the form-finding method developed specifically for gridshells: the improved Multi-body Rope Approach (i-MRA). The i-MRA method builds on the Multi-body Rope Approach (MRA) [29], a form-finding technique used in structural engineering

for designing complex shell and gridshell structures.

In MRA, a structure is represented as a network of masses connected by flexible ropes or cables. This allows for the definition of the geometry of the structure by minimizing bending moments and stresses [40]. The MRA approach defines the structural geometry by minimizing the eccentricity of applied compression forces [41].

The i-MRA method improves on MRA by integrating techniques that optimize the structural geometry for both structural reasons and automation of the construction process. There are two main improvements to i-MRA:

- Multiple Orders MRA (MO-MRA): groups structural elements with identical lengths, reducing the number of types of structural components required for construction.

- Repulsive Nodes MRA (RN-MRA): applies a repulsive force field to the dynamic model, which allows for minor adjustments to the geometry to reduce the number of structural components required.

Implemented in MATLAB, i-MRA provides a powerful tool for generating optimal structural geometries with minimal bending moments and stress. It also reduces the types of structural components required for construction, leading to lower production costs, encouraging mass production, and reducing expenses related to construction management.

The i-MRA method has been tested on four examples of increasing complexity, demonstrating its effectiveness in generating optimal structural geometries.

To verify that the geometries obtained by the proposed new method did not have significant structural disadvantages (in terms of internal solicitations) compared with those calculated by pure form-finding methods, a structural analysis of the structures obtained by basic MRA and i-MRA was carried out. For this purpose, finite element analyses were conducted using SOFiSTiK software [42]. Axial force, bending moment, and Von Mises stresses acting on the two structural geometries were compared by imposing a unit load of -1 kN in the vertical direction on each unrestrained structural node. The study assumed that CHS 200 5 profiles and S275 structural steel were used.

The comparison was made in terms of axial force since the structural type studied is mainly subject to this type of internal action. The comparison in terms of bending moment was chosen because form-finding methods typically aim to minimize the bending moment acting on structures. Therefore, it was important to demonstrate that small deviations from the geometry obtained by pure form-finding did not produce significant increases in the acting bending moment.

The paper is organized as follows. In section 2 the basic equation of the MRA method and the i-MRA are introduced. In particular, in sections 2.1 and 2.2 the techniques for the improvement of the MRA method are presented. Then, in section 3 the results of the application of the new method on different case-studies in terms of obtained geometries and structural analyses are reported. Finally, section 4 is focused on the conclusions and some possible future developments of the presented research topic.

2. Methodology

The Multibody Rope Approach (MRA), developed by [29], is an original method for determining the form of gridshell structures, even for highly complex geometries and for any type of forming load. It is specifically designed for gridshell constructions that use free-forms and standardized building elements. MRA utilizes a dynamic model of falling bodies in space and time domains, in which the final equilibrium configuration is calculated iteratively for each node using the D'Alembert's principle. The special feature of the method is to consider structural elements as ropes connecting masses to nodes. The aim of this approach is to generate a geometry that is both structurally optimal and composed of the greatest possible number of parts of identical length. The final equilibrium configuration of the structure is an inverted representation of the hanging net (funicular configuration). Like particle-spring models, MRA assumes that the self-weight of the nodes and the load of the ropes are localized at the nodes. However, MRA differs from these approaches in its use of ropes to model the hanging network. The ropes have a specific slack coefficient that allows for regular forms. In MRA, the system of forces acting on individual nodes is distinct from those in the spring-particle (SP) and dynamic relaxation (DR) methods. Specifically, the rope element exerts forces on the masses so that they do not move apart beyond the prescribed distance, which is precisely the length of the rope. When the distance between the ends is smaller than the predetermined length of the rope (l_{rope}), no force is applied. By defining l as the distance between the two ends of the rope and k as the axial stiffness of the rope, the forces F applied to the end nodes can be expressed as follows:

$$\begin{cases} F_{rope} = 0 & \text{if} \quad l < l_{rope} \\ F_{rope} = k(l - l_{rope}) & \text{if} \quad l \geq l_{rope} \end{cases} \tag{1}$$

Where the length of the rope l_{ji} between the two nodes i and j can be calculated as:

$$l_{ji} = \sqrt{(x_j - x_i)^2 + (y_j - y_i)^2 + (z_j - z_i)^2} \tag{2}$$

In general, the MRA approach aims to minimize axial deformations by assuming extremely high stiffness values. The goal of MRA is to find a geometric configuration that ensures the equilibrium of nodes subjected to external forces and those emerging from the ropes connected to them. Let's consider a generic node i with a mass of m_i in the structural network of nodes and ropes. The node i is connected to a number n_i of other nodes through ropes. If there is an external load p_i acting on node i, the equilibrium equation can be written as:

$$\vec{R}_i = \vec{p}_i + \sum_{j=1}^{n_i} \vec{F}_{rope,ji} + \vec{F}_i^I + \vec{F}_i^{II} = 0 \tag{3}$$

In this equation, the vector $\vec{R}i$ represents the net force acting on node i, which is the sum of several forces including the applied load p_i, the forces transmitted by the ropes connected to the node $\vec{F}rope, ji$, the inertial force $\vec{F}_i^{II}$, and the damping force $\vec{F}_i^I$. The magnitude of the inertial force $\vec{F}_i^{II}$ can be determined using equation (4), which is calculated as the product of the node's mass m_i and the magnitude of the acceleration vector $\vec{a}_i$, with the direction of the inertial force being opposite to the direction of node

acceleration.

$$\vec{F}_i^{II} = -m_i \cdot \vec{a}_i \tag{4}$$

The damping force $\vec{F}_i^I$ is represented by the product of a constant damping coefficient c_i and the velocity vector $\vec{v}_i$ with direction opposite to the direction of the velocity. This relationship is expressed in equation (5).

$$\vec{F}_i^I = -c_i \cdot \vec{v}_i \tag{5}$$

Expressing the position of the generic node i as $\vec{u}_i = (x_i, y_i, z_i)$, the velocity and the acceleration can be obtained by deriving the position in time, as in the relations (6).

$$\vec{v}_i = \dot{\vec{u}}_i = (\dot{x}_i, \dot{y}_i, \dot{z}_i) \qquad \vec{a}_i = \ddot{\vec{u}}_i = (\ddot{x}_i, \ddot{y}_i, \ddot{z}_i) \tag{6}$$

Thus, the equation (3) can be rewritten as in (7).

$$\vec{R}_i = \vec{p}_i + \sum_{j=1}^{n_i} \left\{ k \cdot \vec{F}_{rope,ji} \right\} - c_i \cdot \vec{v}_i - m_i \cdot \vec{a}_i = 0 \tag{7}$$

Finally, the equilibrium equation (7) can be projected in the three space dimensions, obtaining the system of equation (8).

$$\begin{cases} p_{ix} + \sum_{j=1}^{n_i} \left\{ \frac{(x_j - x_i)}{l_{ji}} \cdot F_{rope} \right\} - c_i \cdot \dot{x}_i - m_i \cdot \ddot{x}_i = 0 \\ p_{iy} + \sum_{j=1}^{n_i} \left\{ \frac{(y_j - y_i)}{l_{ji}} \cdot F_{rope} \right\} - c_i \cdot \dot{y}_i - m_i \cdot \ddot{y}_i = 0 \\ p_{iz} + \sum_{j=1}^{n_i} \left\{ \frac{(z_j - z_i)}{l_{ji}} \cdot F_{rope} \right\} - c_i \cdot \dot{z}_i - m_i \cdot \ddot{z}_i = 0 \end{cases} \tag{8}$$

The system of equations can be solved by considering a time increment of Δt. The positions of the nodes at time $t = 0$ are assumed to be known,

and initial velocities and accelerations are assumed to be zero for each node i ($v_i(0) = 0$ and $a_i(0) = 0$). By knowing the position, velocity, and acceleration of each node at time t, these quantities can be determined at the next instant, $t + \Delta t$. To do so, a coefficient C_3 can be defined as a function of the known node positions at time t^*, as shown in equation (9).

$$C_3 = \vec{p}_i + \sum_{j=1}^{n_i} \left\{ k \cdot \vec{F}_{rope,ji} \right\} \tag{9}$$

The coefficient C_3 depends solely on the position of the nodes at time t^*, and it defines the vector F_{rope}. Consequently, Equation (7) can be reformulated as shown in (10).

$$\ddot{\vec{u}} + \frac{c}{m}\dot{\vec{u}} = C_3 \tag{10}$$

In addition, the natural frequency of the system ω_n and critical damping ζ can be defined as in the equations (11) and (12).

$$\omega_n = \sqrt{\frac{k}{m}} \tag{11}$$

$$\zeta = \frac{c}{2\omega_n m} \tag{12}$$

where k is the stiffness, m is the mass, and c is the damping coefficient of the system. The natural frequency ω_n represents the frequency at which the system vibrates when it is not subjected to any external forces. The critical damping ζ is the damping coefficient value that results in the system being critically damped, which means that it returns to its equilibrium state

as quickly as possible without oscillating. Thus, a non-homogeneous second-order differential equation is obtained:

$$\ddot{\vec{u}} + 2\omega_n \zeta \dot{\vec{u}} = C_3 \tag{13}$$

The solution to the equation (13) can be obtained by adding the particular solution to the associated homogeneous differential equation, which is expressed as (14).

$$\vec{u}(t) = C_1 e^{-2\omega_n \zeta} + C_2 + \frac{C_3}{2\omega_n \zeta} t \tag{14}$$

The coefficients C_1 and C_2 can be calculated based on the initial conditions of the system. In this case, they can be obtained by using the positions and velocities of the nodes at the immediately preceding instant $t - \Delta t$, as shown in the following equations:

$$C_1 = -\frac{2\omega_n \zeta \dot{\vec{u}}_{(t-\Delta t)} - C_3}{(2\omega_n \zeta)^2} \tag{15}$$

$$C_2 = -\frac{(2\omega_n \zeta)^2 \vec{u}_{(t-\Delta t)} + 2\omega_n \zeta \dot{\vec{u}}_{(t-\Delta t)} - C_3}{(2\omega_n \zeta)^2} \tag{16}$$

The coefficients C_1, C_2, and C_3 in the solution depend on the positions, velocities, and accelerations of the system's nodes at the previous time instant. Starting from the initial state where the location of the nodes in the three-dimensional space is known and velocity and acceleration are zero, the positions of the nodes at succeeding instants can be calculated progressively. The velocity vector $\dot{\vec{u}}_t$ can be obtained by taking the difference between the positions of the nodes at instants $t - \Delta t$ and t, and dividing by the time increment Δt:

$$\dot{\vec{u}}_t = \frac{\vec{u}_t - \vec{u}_{t-\Delta t}}{\Delta t} \tag{17}$$

Finally, the acceleration $\ddot{\vec{u}}_t$ can be determined by computing the ratio of the incremental change in velocity between two time instants $t - \Delta t$ and t. Specifically, this can be achieved by calculating the difference between the two velocities and dividing it by the time interval Δt.

$$\ddot{\vec{u}}_t = \frac{\dot{\vec{u}}_t - \dot{\vec{u}}_{t-\Delta t}}{\Delta t} \tag{18}$$

The proposed method is designed to calculate the final configuration of a gridshell from its initial mesh, which represents the initial state of the net. Since the initial position of nodes is known, and their initial velocities and accelerations are assumed to be zero, the new locations, velocities, and accelerations of nodes can be determined sequentially using equations (14), (17), and (18). This process is repeated until an equilibrium configuration is reached that represents the optimal structural geometry with respect to the applied force field $\vec{p}$. The estimated structural geometry is a function of various parameters, including the nodal masses m, the system stiffness k, damping parameters c, the rope slack coefficient ρ, and the applied force field $\vec{p}$. The slack coefficient ρ is defined as the ratio of the initial distance between nodes to the target length of the ropes, as shown in equation (19).

$$\rho_{ij} = \frac{l_{rope}}{\vec{u}_i(0) - \vec{u}_j(0)} = \frac{l_{rope}}{\sqrt{(x_i - x_j)^2 + (y_i - y_j)^2 + (z_i - z_j)^2}} \tag{19}$$

The objective of applying MRA is to generate a structural geometry that is optimal in terms of both structural effectiveness and ease of construction.

To evaluate the ease of construction, the number of beam elements of equal length is used as a measure. In practice, the complexity of gridshell assembly increases exponentially as the number of different elements to be assembled grows. Therefore, it is crucial to determine the number of elements in the final configuration that have a length equal to the target length l_{rope}, while considering a certain tolerance $toll$. Based on their length, structural elements are classified into three categories: those with a length less than l_{rope} are called *loose elements*, those with a length greater than l_{rope} are called *over elements*, and those with a length equal to l_{rope} are referred to as *target elements*. The presence of *over elements* can be reduced or eliminated by appropriately choosing the model parameters, including the stiffness coefficient k, the slack coefficient ρ, and the time interval Δt. In contrast, the presence of *loose elements* is determined by the physics of the problem and arises from ropes that do not experience tension as a result of the applied force field.

This paper introduces two methods, Multiple Orders MRA (MO-MRA) and Repulsive Nodes MRA (RN-MRA), that can be used to reduce the number of *loose elements* obtained through MRA. These methods can be applied after MRA to update the final configuration, resulting in a structure with fewer components of different lengths, making it easier to assemble. When combined, these methods are referred to as Improved MRA (i-MRA), which, with a wise selection of model parameters and target lengths, can produce geometries that are both structurally effective and optimal in terms of ease of fabrication.

2.1. Multiple Orders MRA

The Multiple Order MRA is a method that aims to reduce the number of different structural elements obtained by using classical MRA. The structural geometry obtained by applying MRA will be defined by a number of structural elements of length $l_{rope,1}$ and the remaining *loose elements*. The use of MO-MRA involves introducing new families of ropes each characterized by a length shorter than $l_{rope,1}$. The assignment of each rope to each family will be determined for each iteration and will be defined as a function of the distance between the two nodes connected by the rope. After the geometric configuration using the MRA is obtained, consider adding a new family of ropes with a final length of $l_{rope,2} < l_{rope,1}$. In this scenario, the force $\vec{F}_{rope}$ exerted by each rope will depend on the family to which it belongs, and as a result, it will be a function of the distance between the two nodes connected by the rope. In particular, $\vec{F}_{rope}$ can be calculated as in the equation 20.

$$\begin{cases} F_{rope} = 0 & \text{if} \quad l < l_{rope,2} \\ F_{rope} = k(l - l_{rope,2}) & \text{if} \quad l_{rope,2} < l \leq \gamma(l_{rope,1} - l_{rope,2}) + l_{rope,2} \\ F_{rope} = 0 & \text{if} \quad \gamma(l_{rope,1} - l_{rope,2}) + l_{rope,2} < l < l_{rope,1} \\ F_{rope} = k(l - l_{rope,1}) & \text{if} \quad l \geq l_{rope,1} \end{cases} \tag{20}$$

The resulting equilibrium configuration is iteratively calculated using equations (14), (17), and (18) and will correspond to a new structural geometry. In the new configuration, the structural element will belong to three different element groups, the two characterized by the target lengths $l_{rope,1}$ and $l_{rope,2}$, and, eventually, the third group composed by the *loose el-*

ements. The procedure can be repeated adding new families of ropes until all structural elements correspond to an assigned category. The proposed method reduces the cost and complexity associated with the construction of gridshells by grouping structural components with the same length, which enables the possibility of producing the elements in series and facilitates the ease and speed of the structure's construction. On-site management of the groups of elements is simple and straightforward.

The MO-MRA method offers users the flexibility to set parameters such as the coefficient and rope lengths ($l_{rope,2}$, $l_{rope,3}$, etc.) to tailor the structural geometry to their design needs. These parameters are user-defined and allow for the optimization of the structural design to meet specific construction or manufacturing constraints. For instance, $l_{rope,1}$, defining the first family of structural elements, can determine the structure's height (see Figure 3). However, in cases where cutting steel billets of a constant length is involved, setting $l_{rope,1}$ may lead to material wastage. Therefore, the lengths of other structural element families can be adjusted to minimize waste. Similarly, the coefficient γ plays a crucial role in assigning the ropes that remain slack, after the application of the MRA, to different structural element families. It determines the proportion of ropes with intermediate lengths between the target lengths of two families that are assigned to each family. The process of defining the final structural geometry involves configuring both γ and the target lengths for each family, which can vary widely depending on each project's unique requirements. An alternative approach is to create an objective function based on specific design requirements. This allows for the formulation of an optimization problem, where the mentioned parameters

become design variables. By applying optimization algorithms to solve this problem, it is possible to automatically obtain parameter values that best align with the design requirements [43].

2.2. Repulsive Nodes MRA

The Repulsive Nodes MRA is a method designed to reduce the number of *loose elements* generated by applying the basic MRA. The basic idea is to introduce a repulsive force field $\vec{q}$ between the nodes of the geometric configuration obtained through the use of MRA. This force field $\vec{q}$ is introduced after the final equilibrium configuration is established using the MRA, which requires a new iterative computation process to determine the new equilibrium condition. The repulsive forces act on the ends of each slack rope, allowing the end nodes to move apart as if they possess electrical charges of the same sign that repel each other until the rope tensioning. Therefore, for each node connected by a slack rope, Equation (7) must be modified by introducing the repulsive force field $\vec{q}$. As a result, a new system of equations will be obtained in which equation (7) will continue to apply for nodes connected to tensioned ropes, and equation (21) will be introduced to each node i connected to slack ropes.

$$\vec{R}_i = \vec{p}_i + \vec{q}_i + \sum_{j=1}^{n_i} \left\{ k \cdot \vec{F}_{rope,ji} \right\} - c_i \cdot \vec{v}_i - m_i \cdot \vec{a}_i = 0 \tag{21}$$

Equation (21) introduces the repulsive force field $\vec{q}$ to each node i connected to slack ropes. This force field $\vec{q}$ is linearly proportional to the difference between the target length l_{rope} and the distance between nodes connected by a slack rope l_{ij}. To calculate the repulsive force field $\vec{q}$, Equation

(22) can be used, where k_{rep} is the proportionality constant that connects the modulus of the repulsive force to the distance between nodes i and j.

$$q_i = -k_{rep}(l_{rope} - l_{ij}) \tag{22}$$

The value of the elastic coefficients k and k_{rep} depends on many factors. For example, the coefficient k must be selected depending on the length of the ropes, the applied loads, the value of the nodal masses, the time interval Δt defining each iteration, etc. The elastic coefficient k must be big enough to avoid the presence of *over elements* and, at the same time, not so big as to ensure convergence of the system. For the application cases reported in this paper, a k value of $1.2MN/m$ with a $\Delta t = 0.005s$ was used. These values can be considered as a starting point for different applications. The procedure involves to increase the value of k until no more *over elements* are present in the final configuration and consequently to reduce Δt in case the system does not reach the convergence status. Similarly, the value of k_{rep} must be selected so that repulsive forces between nodes do not produce *over elements* in the final geometric configuration. In the case studies presented in this work, a k_{rep} of $2kN/m$ was used, which can also be used as a first attempt value for applications other than those presented.

It should be noted that the force field introduced in RN-MRA is not a representation of the actual loads on the structure. Therefore, the resulting structural shape may differ from the optimal solution obtained through the pure form-finding process. While the RN-MRA method improves the constructability of the structure, it may also result in suboptimal and unattractive shapes, particularly when applied to models with a significant number of

loose elements, as shown in Figure 11. Therefore, it is important to apply the RN-MRA method only to apply minor changes to the geometry obtained by applying the MO-MRA in order to strike a balance between enhancing constructability and achieving the best structural geometry. Ideally, RN-MRA should be applied to models with few *loose elements* relative to the number of tensioned ones, and where their length is close to the target length l_{rope}.

In this section, two MRA advances are discussed to produce structural solutions that are more advantageous in terms of construction convenience. The i-MRA technique combines these approaches to achieve a geometry with the optimal balance of structural functionality and ease of construction. The first approach involves increasing the families of elements in the MO-MRA until a configuration is obtained in which most of the ropes are under tension. The second approach, RN-MRA, is then used to improve the geometry by tensioning the remaining loose elements. As a result, the final shape may differ slightly from the geometry obtained using MO-MRA alone, but it is characterized by the smallest possible number of *loose elements*.

An example of how the structural geometry evolves gradually from the shape generated using only MO-MRA initially and then the combination of MO-MRA and RN-MRA is shown in Figure 20. Here, you can observe how the two newly introduced methods take effect collaboratively to reduce the number of structural components with varying lengths.

3. Application and results

In this section, four applications of the proposed method on structural geometries of increasing complexity are presented. A custom Matlab code

[44] was developed for applying the proposed methods. The geometries are represented as quadrilateral meshes where the nodes have a concentrated mass and the edges are ropes that connect the nodes. The MRA is applied to each mesh to produce the equilibrium configuration, which represents the final structural form. By varying the method parameters, different structural shapes are generated, and the variation of the geometries and the number of equal elements as a function of the slack coefficient is studied. It is observed that appropriate parameter selection, especially in the setting of the correct time interval, allows for the reduction and elimination of *over elements*. Finally, the structures generated by the various form-finding algorithms discussed in section 2 are compared in terms of structural analysis as well as the number of structural components of equal length that constitute the structure. The comparison shows that the i-MRA allows for reducing the costs related to the realization of gridshell structures while respecting the structural optimal solution produced by a pure form-finding method. Overall, the proposed method is shown to be effective in producing structural solutions that are both functional and easy to construct.

3.1. Application 1: Corner constrained square-plan structure

The structural geometry of a square gridshell is defined using the MRA method applied to a square mesh with a side of 15 meters and lines placed in an orthogonal grid linking nodes at a distance of $l_{ij} = 1.25m$, as shown in Figure 2. The structure is designed to be constrained only in the corners of the square plan, and the constraints are represented as triangular points in Figure 2.

Although this is a basic case study from a theoretical perspective, the

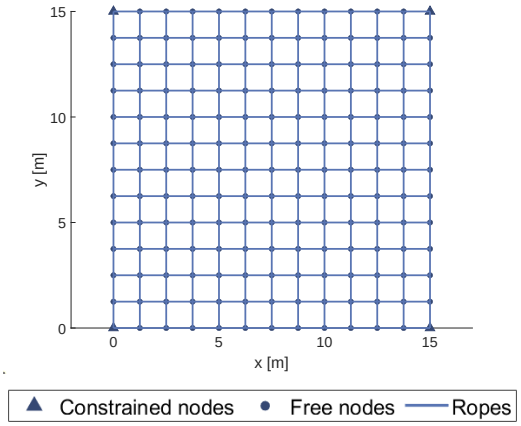

Figure 2: Base mesh for corner constrained square-plan structure

Parameters MRA				
$K[MN/m]$	$m[kg]$	$\zeta[s^{-1}]$	$\Delta t[s]$	$iter_{max}[/]$
1.2	20	0.95	0.005	100000

Table 1: MRA parameters.

structure is demonstration of the ability of this structural typology to generate constructively complex shapes from the simplest of forms. The resulting structure is composed of 312 structural elements and 169 nodes. By using an appropriate parameter setting, as detailed in Table 1, it is possible to obtain a structural geometry where all beam elements have the same length, with a tolerance of one centimeter.

The ratio of the maximum horizontal structural dimension to the height of the structure is referred to as the degree of sag, denoted as η. By varying the slack coefficient ρ, it is possible to generate different structural shapes with varying degrees of sag. The relationship between the degree of sag η and the slack coefficient ρ for the specific geometric configuration examined

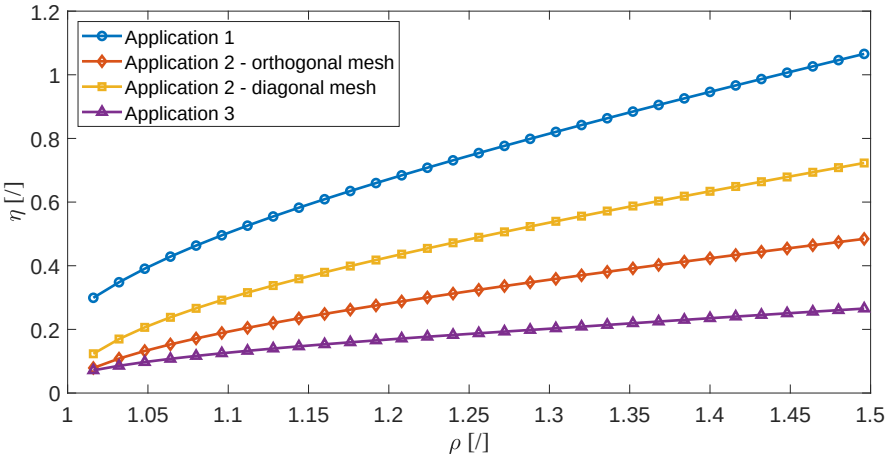

Figure 3: Degree of sag η as function of the slack coefficient ρ

in this section is illustrated in Figure 3. The graph clearly indicates that for values of $\rho > 1.1$, the height of the structure increases in proportion to the slack coefficient. The graph can be utilized by designers to determine the target length l_{rope} as a function of the design structural height.

Figure 4 displays four different geometric configurations that can be generated from the same basic mesh, each having a distinct slack coefficient ρ and consequently a different height. It is noteworthy that having the ability to produce several geometries from a single basic plan is crucial. The choice of a specific geometric form over another may be influenced by various factors, such as architectural or structural considerations. The parameters utilized to create the different structural geometries are listed in Table 1. It is evident that each geometric configuration necessitates a specific number of iterations $iter$, and the more the final configuration varies from the initial one, the more iterations are needed. Therefore, higher structures require more iterations and, as a result, longer computation times.

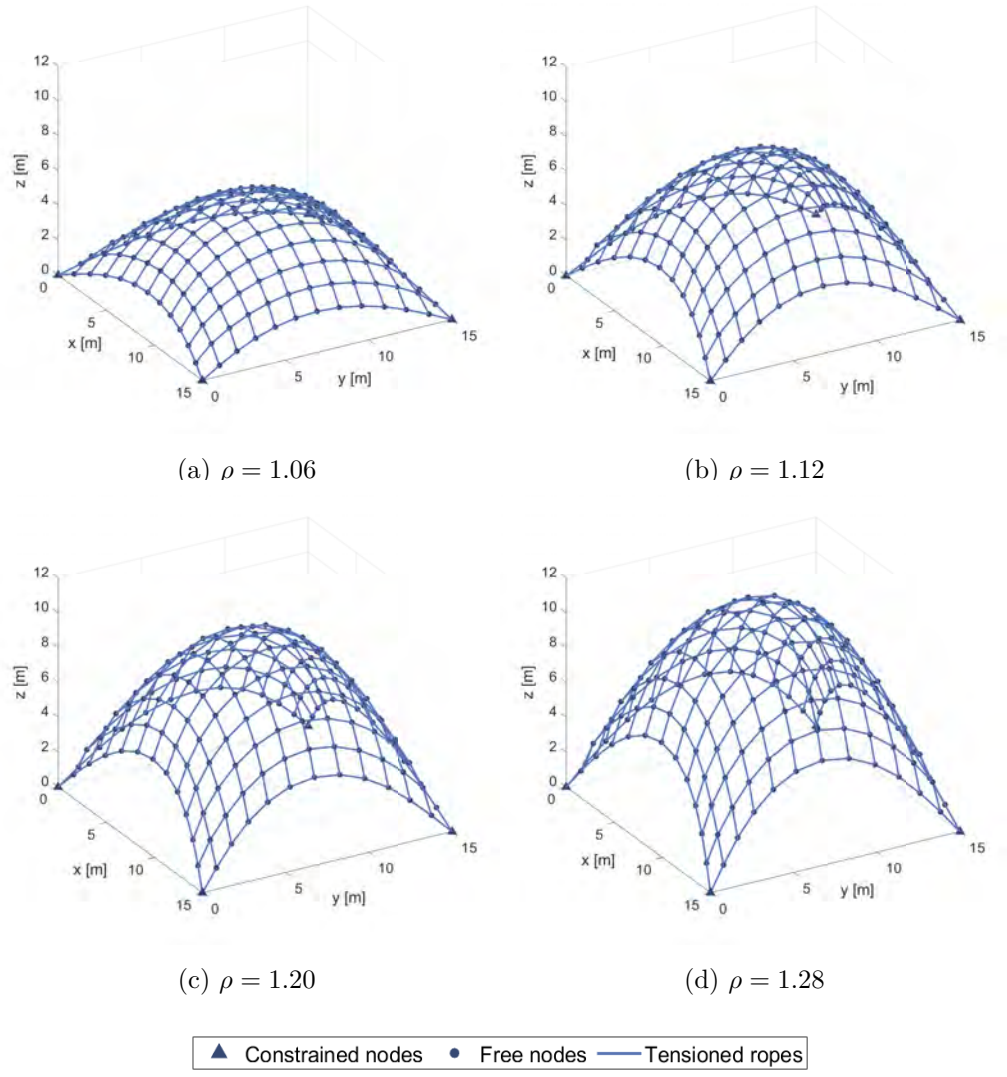

(a) $\rho = 1.06$ (b) $\rho = 1.12$

(c) $\rho = 1.20$ (d) $\rho = 1.28$

Figure 4: MRA application on corner constrained square-plan structure for different slack coefficients ρ.

3.2. Application 2: Boundary constrained square-plan structure

In the second scenario, a square mesh with a side length of 15 meters was used, which is similar to the one shown in Section 3.1. However, in this case study, all points on the mesh's edge were constrained, unlike the previous scenario. This means that there are fewer options to adapt the final design due to the increased restrictions placed on the structure. Despite this, the MRA method alone still enabled designs with a significant proportion of structural components having the same length. The method's robustness was demonstrated by creating two different starting configurations from the same edge constraints. The first configuration used a square grid mesh with perpendicular elements connecting nodes at a distance of $1.25m$, as shown in Figure 5*a*. In the second case, the mesh was constructed by connecting the constrained nodes on the edges with diagonal elements, resulting in a final mesh with more nodes and structural components, as shown in Figure 5*b*. The two meshes differ significantly in terms of node and component quantity and layout. The first case has 165 nodes and 264 elements arranged parallel to the base square's sides, while the second case has 313 nodes and 576 elements aligned at a 45° angle.

The figures presented in Figure 7 illustrate four examples of structural geometries that were derived from the same basic mesh in Figure 5*a*. By varying the slack coefficient ρ, it is apparent that even minor increases in structural complexity, which are solely determined by the arrangement of constraints, make it impossible to achieve 100 percent equal-length structural elements using the basic MRA. The structural components with lengths that differ from the target length L_{rope} are highlighted in red in Figure 7.

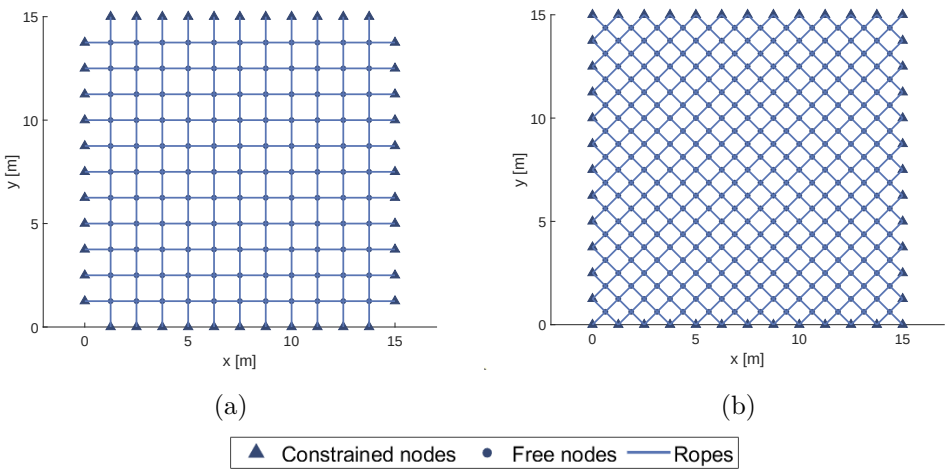

Figure 5: Base mesh for boundary-constrained square-plan structure

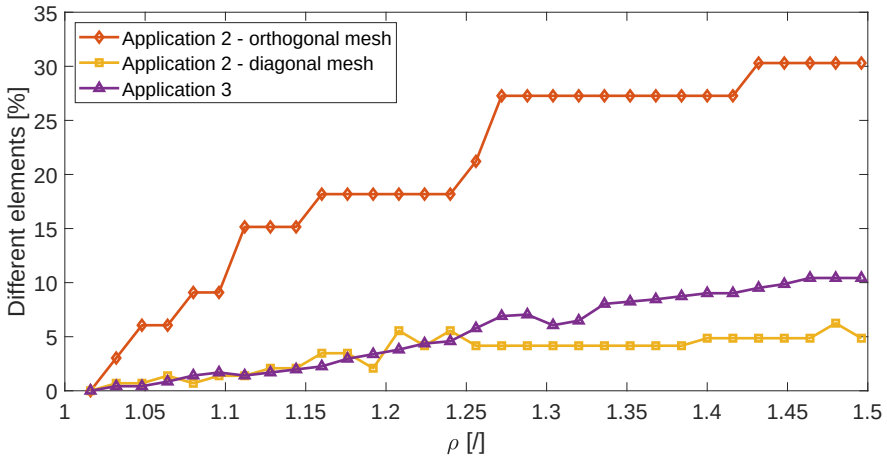

Figure 6: Percentage of loose ropes as a function of the slack coefficient ρ

Parameters RN-MRA		
$K[kN/m]$	$\Delta t[s]$	$iter_{max}[/]$
2.0	0.005	3000

Table 2: RN-MRA parameters

The graph in Figure 6 illustrates how the number of different elements increases proportionally to the slack coefficient ρ. When $\rho = 1.5$, 30% of elements have lengths different from the target one. However, due to the simple and symmetrical nature of the initial geometry, managing the presence of these elements during construction should be straightforward. Despite the simple geometry, the provided example demonstrates that *loose ropes* can be generated using the basic MRA. For instance, in Figure 7*c*, which has $\rho = 1.20$, the structure comprises 6 different structural elements, even considering the structural symmetry. Nearly 20% of elements have a length $l \neq 1.50m$. In such cases, the usage of i-MRA can help reduce the number of different structural components. Figure 9 shows the application of i-MRA to calculate the structure in Figure 7*c*. The use of i-MRA with the slack coefficients $\rho = (\rho_1; \rho_2; \rho_3)$ results in a structure comprising only three different structural element types. Table 2 reports the parameters used to apply the repulsive nodes MRA (RN-MRA).

In the geometry depicted in Figure 9*a*, where the slack coefficients are set to $\rho = (1.20; 1.12; 1.06)$, every element has a length of either 1.5, 1.4, or 1.3 meters, demonstrating the clear advantages of using i-MRA. Even in this relatively simple scenario, the method allows for a reduction in the number of element types from 6 to just 3, resulting in 50% reduction in the

number of element types that need to be managed during construction, even when considering a precision of just one centimeter. Figure 9*b* presents the results of applying i-MRA to the same structural scenario but with different slack coefficients set at $\rho = (1.20; 1.08; 1.00)$. This configuration generated a structure composed exclusively of elements measuring 1.50, 1.35, or 1.25 meters in length, and once again, only three different structural element types were required. This further highlights the versatility of i-MRA in allowing designers to customize the parameters to achieve various configurations that meet project requirements without increasing the complexity of construction.

Histograms were employed to illustrate the distribution of element lengths, aiming to enhance understanding of the variation in the quantity of different types of structural elements. Specifically, Figure 8 presents the distributions of element lengths for the case studies depicted in Figure 7. The histograms clearly demonstrate how both the types of structural elements and their lengths increase with the rise in the slack coefficient. Additionally, Figure 10 illustrates the distribution of element lengths corresponding to the cases depicted in Figure 9. In this case, it is evident that the use of the i-MRA results in a significant reduction element typologies.

An example of misapplication of the method is shown in Figure 11. In this case, the RN-MRA method was applied directly after MRA, without utilising MO-MRA as an intermediate step. The geometry obtained through MRA had excessive *loose elements*, making it unsuitable for direct application of RN-MRA. The result is a geometry that does not find a good balance of convenience in construction and structural efficiency.

Figure 12 displays four examples of basic MRA applied to the base mesh

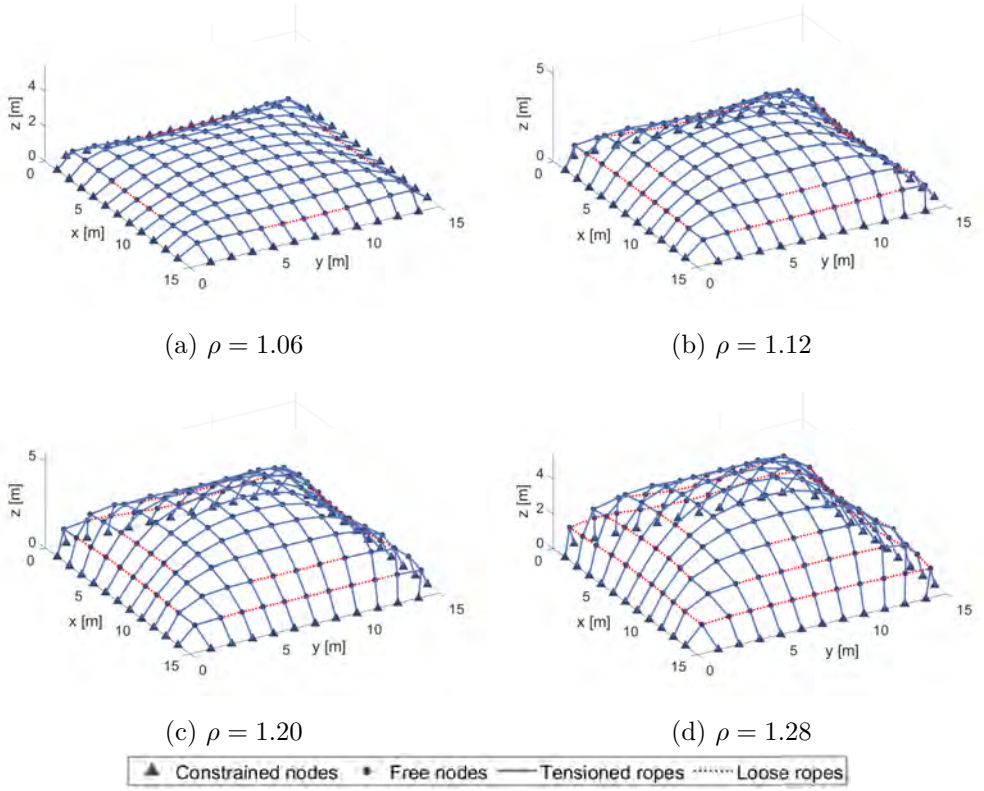

(a) $\rho = 1.06$ (b) $\rho = 1.12$

(c) $\rho = 1.20$ (d) $\rho = 1.28$

Figure 7: MRA application on boundary constrained square-plan structure with orthogonal mesh, for different slack coefficients ρ.

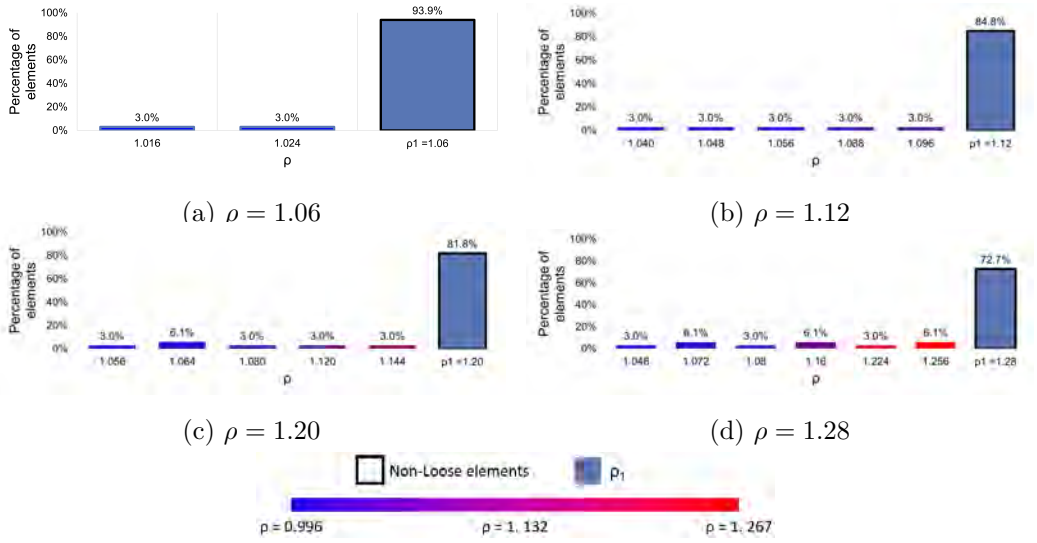

(a) $\rho = 1.06$ (b) $\rho = 1.12$

(c) $\rho = 1.20$ (d) $\rho = 1.28$

Figure 8: Application 2 with orthogonal base mesh: Structural element lengths distribution applying the MRA.

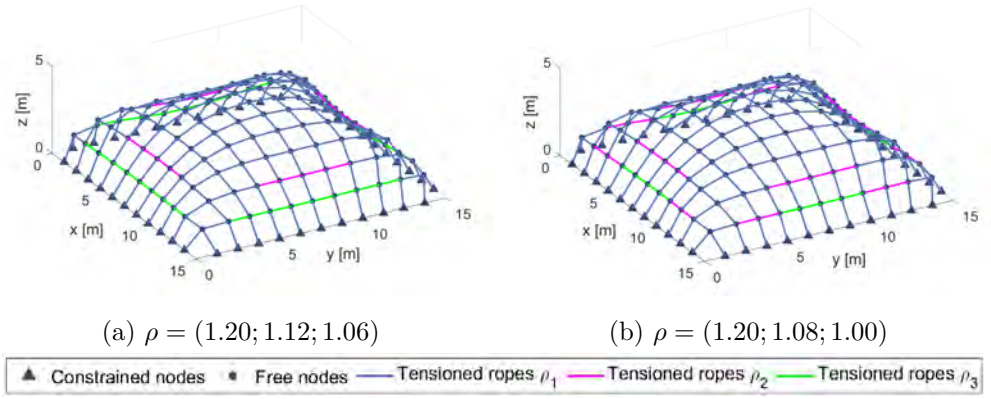

(a) $\rho = (1.20; 1.12; 1.06)$ (b) $\rho = (1.20; 1.08; 1.00)$

Figure 9: i-MRA application on boundary constrained square-plan structure with orthogonal mesh for different slack coefficients ρ.

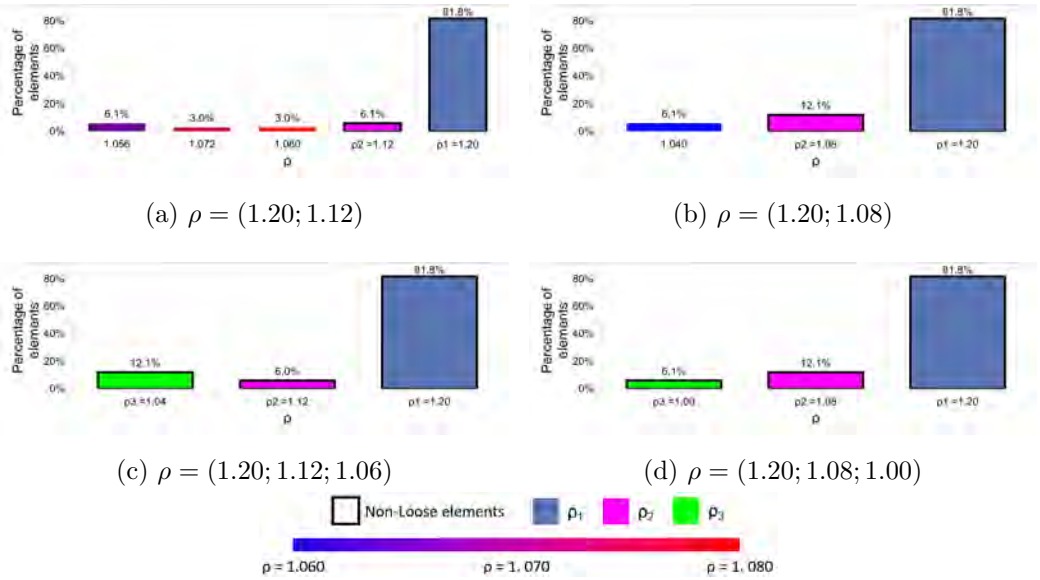

(a) $\rho = (1.20; 1.12)$ (b) $\rho = (1.20; 1.08)$

(c) $\rho = (1.20; 1.12; 1.06)$ (d) $\rho = (1.20; 1.08; 1.00)$

Figure 10: Application 2 with orthogonal base mesh: Structural element lengths distribution applying the i-MRA.

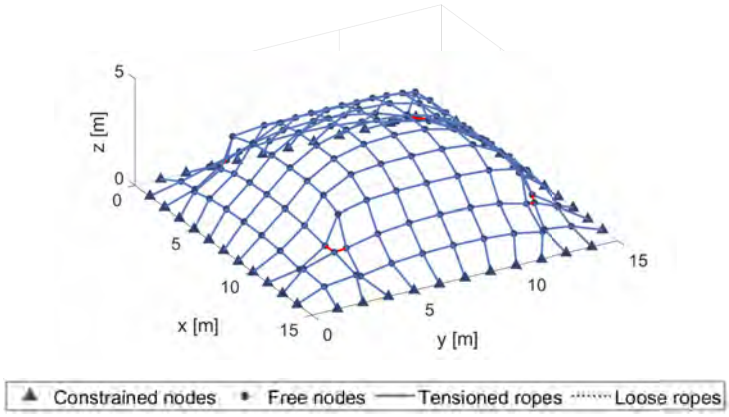

Figure 11: Incorrect application of RN-MRA application on boundary constrained square-plan structure with orthogonal mesh and $\rho = 1.20$.

from Figure 5*b*, generated by varying the slack coefficient. It is clear from this scenario that the resulting structures differ greatly from those in the previous case, both in terms of shape regularity and degree of sag η. The degree of sag η is plotted as a function of the slack coefficient ρ in the graph in Figure 3. The function trend is identical to that obtained with other basic geometries, but the obtained values here are quantitatively different. Diagonal gridshells are typically higher than those produced by the orthogonal mesh with the same slack coefficient. Additionally, Figure 6 reports the percentages of elements that differ from the target ones after applying basic MRA. In this scenario, the number of different elements out of the total is evidently smaller than in the previous case, with a maximum of 5% compared to the previous maximum of 30%. Moreover, for specific slack coefficient values, privileged configurations are revealed. The function representing the percentage of different elements as a function of the slack coefficient presents local minima for certain values of ρ, which may be advantageous from a design perspective as they enable the reduction of the number of different structural element classes. Comparing the cases presented in this section, it is evident that the choice of mesh and initial parameters is critical to the final design output. A good initial choice of parameters can have a great influence on the final structural geometry, regardless of the form-finding method used to calculate it. In Figure 13, the distribution of element lengths is illustrated for the case studies with different slack coefficients depicted in Figure 12. This figure highlights once again that increasing the slack coefficient ρ results in an increase in the number of element typologies.

The application of i-MRA to the geometry with $\rho = 1.20$ provided in Fig-

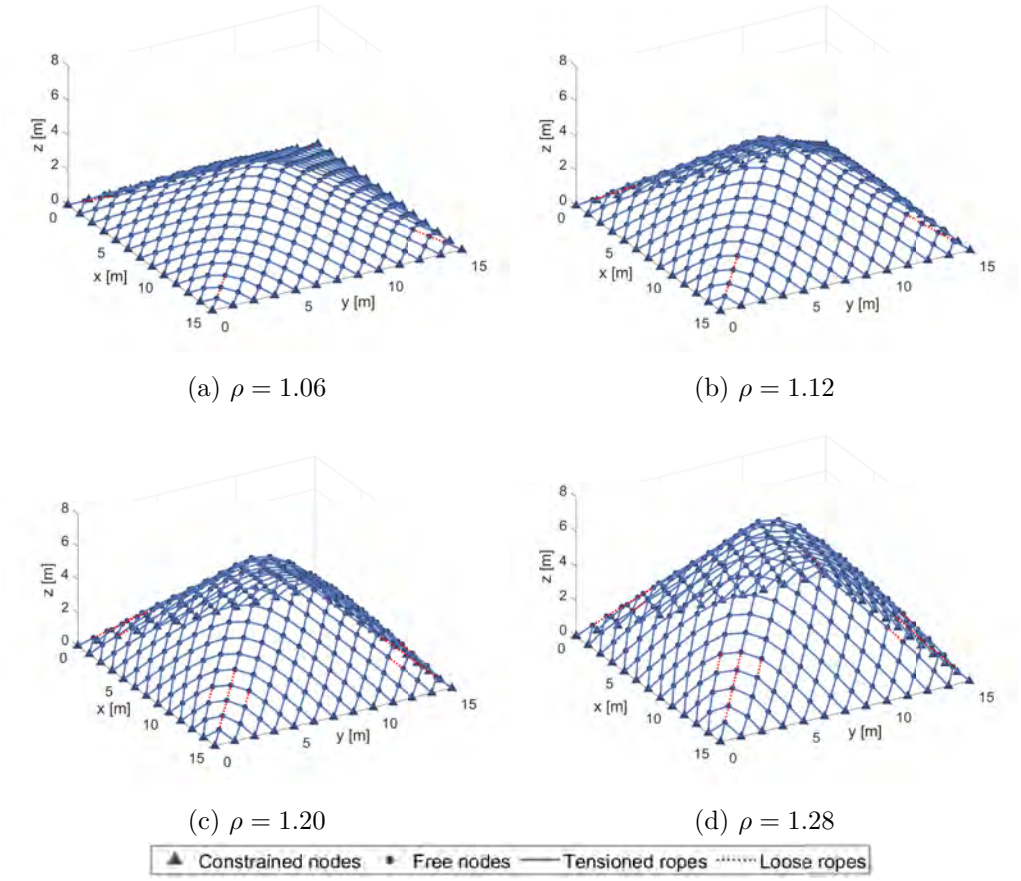

(a) $\rho = 1.06$ (b) $\rho = 1.12$

(c) $\rho = 1.20$ (d) $\rho = 1.28$

Figure 12: MRA application on boundary constrained square-plan structure with diagonal mesh, for different slack coefficients ρ.

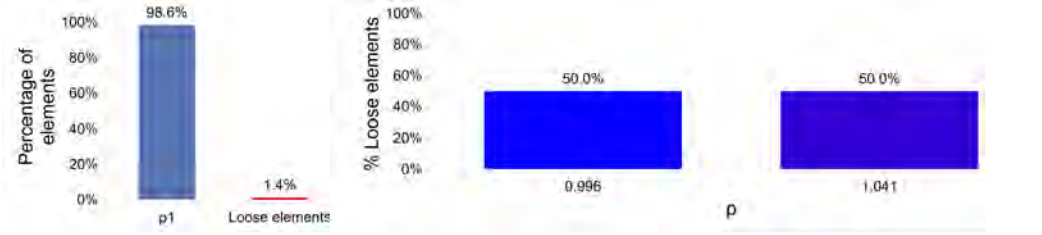

(a) $\rho = 1.06$

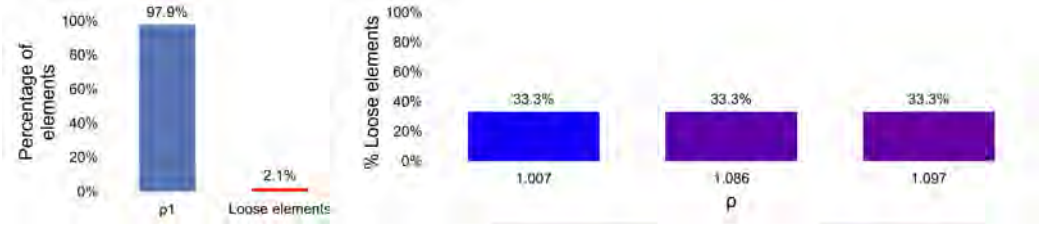

(b) $\rho = 1.12$

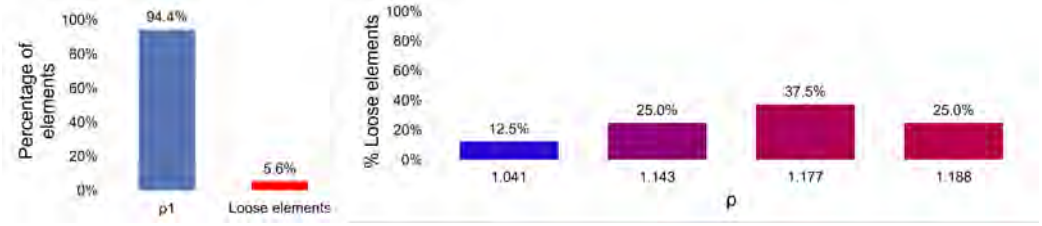

(c) $\rho = 1.20$

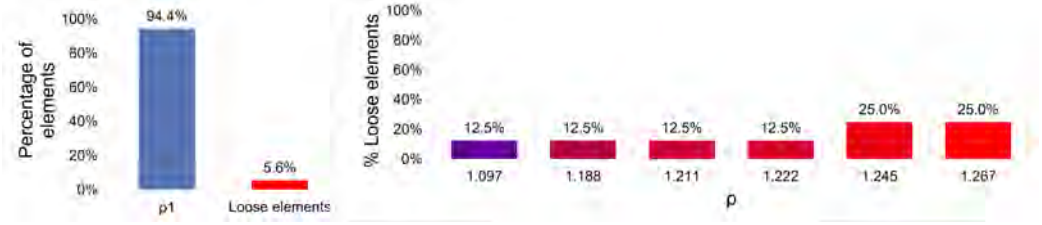

(d) $\rho = 1.28$

Figure 13: Application 2 with diagonal base mesh: Structural element lengths distribution applying the MRA.

ure 12c is presented in Figure 14. The geometry produced by the basic MRA results in 5 different types of structural elements assuming structural symmetry is taken into account. However, the i-MRA approach allows for reducing the variety of structural elements even in this straightforward situation. The gridshell calculated with the i-MRA and slack coefficient $\rho = (1.2; 1.09)$ can be realized using only 2 types of structural elements, demonstrating the effectiveness of the newly presented method in reducing the variety of elements to be handled during the construction process. Additionally, in Figure 14a, it is highlighted that using only MO-MRA allows for obtaining a geometry composed of 3 types of elements. The power of i-MRA can be further appreciated by obtaining a structure composed of only two types of elements through the wise use of RN-MRA properly combined with MO-MRA, as shown in Figure 14b. The reduction in the number of element typologies resulting from the application of i-MRA is evident in Figure 23, where the distribution of element lengths is represented by the mean of histogram graphs.

Figures 16 and 17 present a comparison of the structural analysis results obtained with basic MRA and i-MRA methods for S275 structural steel gridshells composed of *CHS 200 5* profiles and loaded on each node with a unity load in the gravitational direction. These figures show, on the left, the analyses conducted on structures obtained with basic MRA and, on the right, those obtained with i-MRA. Specifically, Figure 16 shows the analyses for the configuration shown in Figure 7c on the left, and those for the configuration in Figure 9a on the right. Figure 17 shows the analyses of the structure in Figure 12c on the left, and the analyses of the structure in Figure 14b on the right. The comparisons in both figures are presented in terms of axial

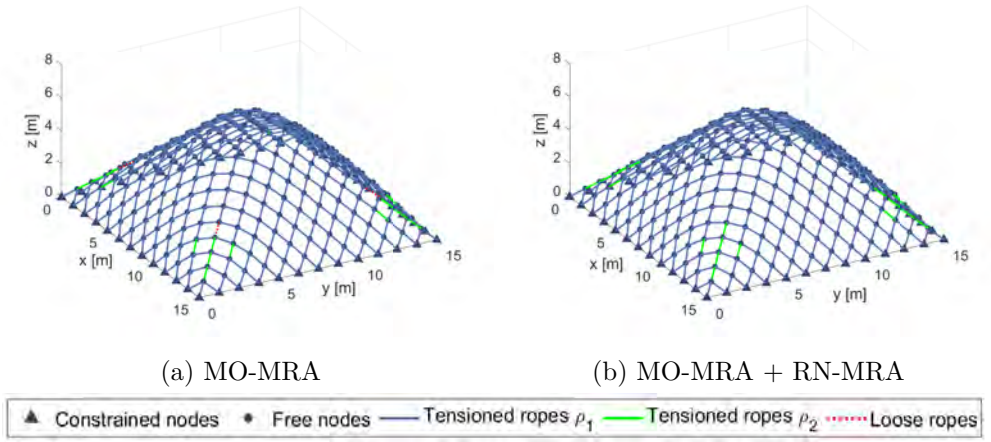

(a) MO-MRA (b) MO-MRA + RN-MRA

Figure 14: i-MRA application on boundary constrained square-plan structure with diagonal mesh.

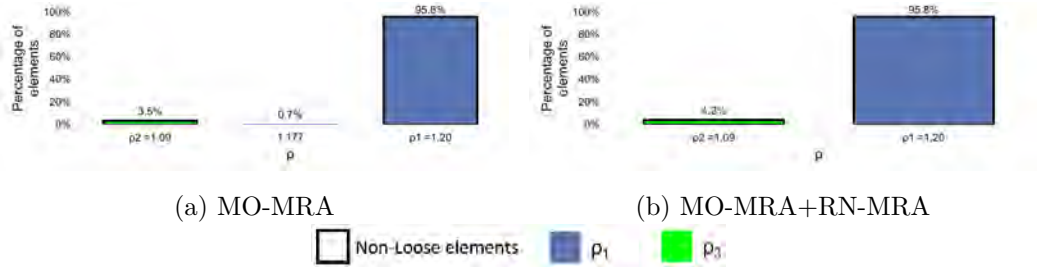

(a) MO-MRA (b) MO-MRA+RN-MRA

Figure 15: Application 2 with diagonal base mesh: Structural element lengths distribution applying the i-MRA.

force at the top, bending moment in the middle, and Von Mises stress at the bottom.

The i-MRA produces geometries that deviate from the funicular structural form. However, the differences in terms of stresses between the i-MRA and basic MRA geometries appear to be minimal. Although the geometries are different, they have similar structural behavior. In the cases presented in this section, the i-MRA produces a significant improvement in terms of minimizing the types of elements that make up the structure. The cost of the geometric variation produced from the viewpoint of structural optimum seems to be small, as demonstrated by the reported comparisons.

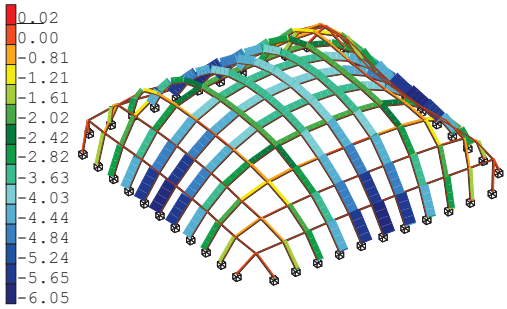

(a) MRA: $|N|_{max} = 6.05kN$

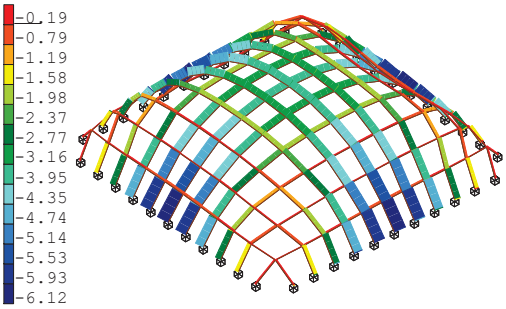

(b) i-MRA: $|N|_{max} = 6.12kN$

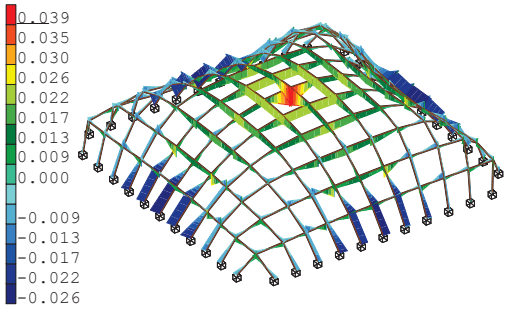

(c) MRA: $|M|_{max} = 0.04kNm$

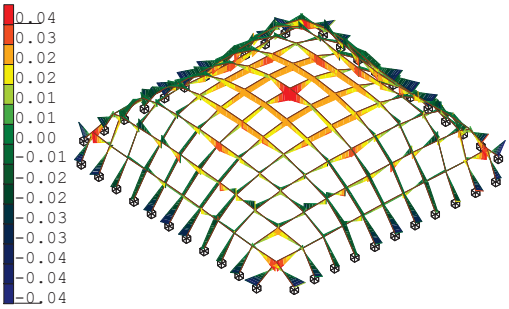

(d) i-MRA: $|M|_{max} = 0.04kNm$

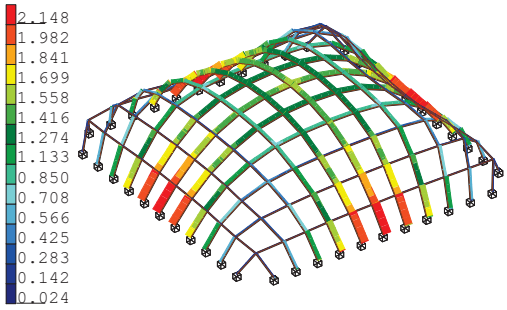

(e) MRA: $|\sigma^{VM}|_{max} = 2.15kPa$

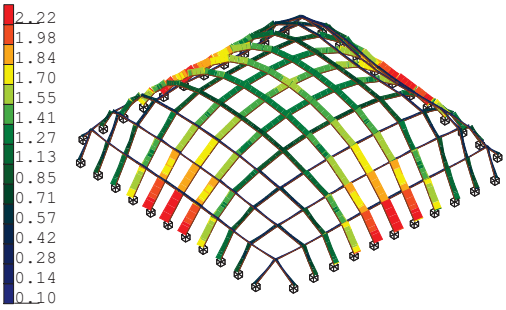

(f) i-MRA: $|\sigma^{VM}|_{max} = 2.22kPa$

Figure 16: Structural analysis performed on the structures obtained by applying basic MRA (left) and i-MRA (right) on the application example with orthogonal mesh in Section 3.2. Comparison in terms of axial force [kN] (top), bending moment [kNm] (middle) and Von Mises stress [kPa] (bottom).

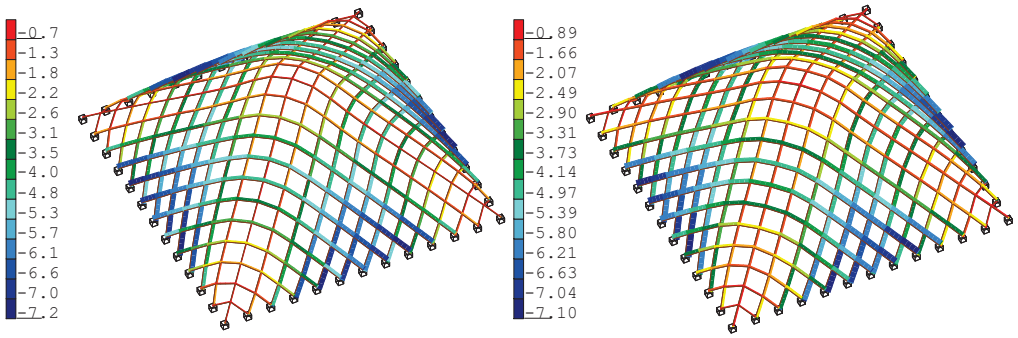

(a) MRA: $|N|_{max} = 7.2kN$ (b) i-MRA: $|N|_{max} = 7.1kN$

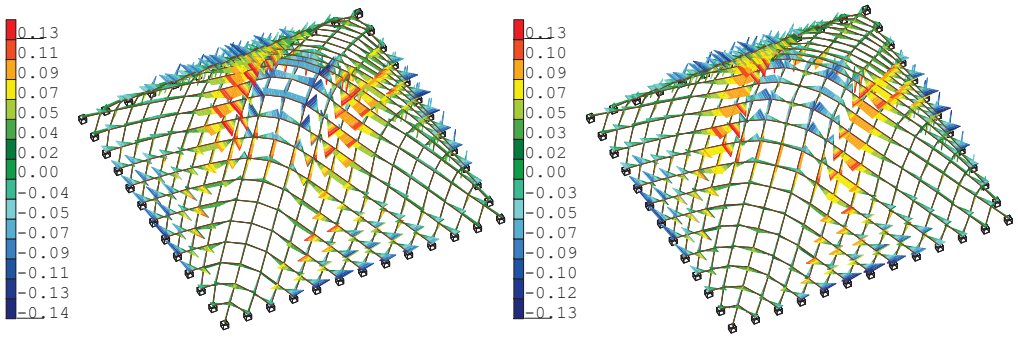

(c) MRA: $|M|_{max} = 0.14kNm$ (d) i-MRA: $|M|_{max} = 0.13kNm$

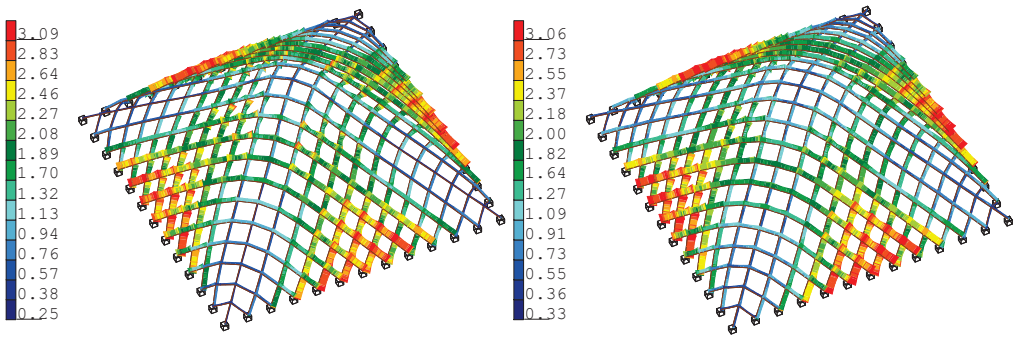

(e) MRA: $|\sigma^{VM}|_{max} = 3.09kPa$ (f) i-MRA: $|\sigma^{VM}|_{max} = 3.06kPa$

Figure 17: Structural analysis performed on the structures obtained by applying basic MRA (left) and i-MRA (right) on the application example with diagonal mesh in Section 3.2. Comparison in terms of axial force [kN] (top), bending moment [kNm] (middle) and Von Mises stress [kPa] (bottom).

3.3. Application 3: Symmetrical structure with a non-canonical geometric plan and opening in the center.

The third example structure features a ground plan that is divided into five primary zones. The main zone is a large rectangular space with a square opening in the center, while four smaller rectangular areas overlap the main one at the corners of the central zone. Figure 18 displays the structure's mesh, which consists of 1419 elements measuring 1.20 meters in length connecting the 760 nodes. The structure is constrained on each outer corner as well as around the entire perimeter of the central hole. This scenario was chosen to introduce some complexity and demonstrate how the approach can handle complex situations. Nevertheless, this structural design has a regular plan characterized by two axes of symmetry. Similar to the previous cases, the relationship between the slack coefficient and the height of the structure, as determined by the form-finding process, was investigated. As depicted in Figure 3, the height trend as a function of the slack coefficient exhibits qualitatively the same behavior as that observed in the simpler examples, even for a complex structural geometry like the one under consideration.

Figures 19 and 20a show four examples of structural geometries obtained with different slack coefficients. It can be observed that the number of *loose ropes*, which corresponds to the number of structural elements of varying lengths, increases as the slack coefficient increases. Figure 6 depicts this trend, revealing that the progression is not monotonically increasing and that there are preferred configurations with a smaller percentage of different elements.

This section effectively demonstrates the potential of i-MRA through

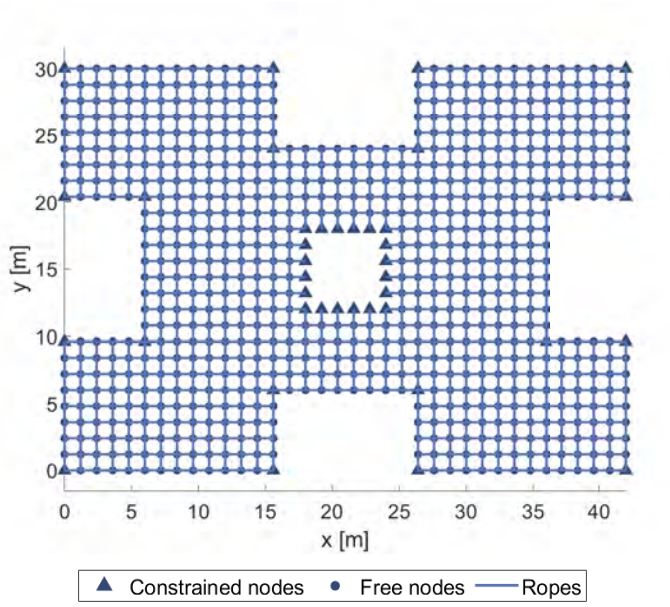

Figure 18: Base mesh symmetrical structure with non-canonical geometric plan and opening in the center.

the analysis of the geometry obtained with a slack coefficient of $\rho = 1.20$, as shown in Figure 20a. The analysis reveals that over 3.5% of the structural elements are shorter than the target length. However, since the entire structure can be completed using only 11 different types of components, the basic MRA is deemed highly efficient. By incorporating structural symmetries and regular initial meshes, the number of required element types can be significantly reduced. Figure 20 illustrates the structural configurations obtained in the successive steps of the i-MRA application. In particular, Figure 20a depicts the application of MO-MRA with two orders of structural elements. This configuration is obtained by setting target lengths $L_{rope} = (1.44m; 1.35m)$, corresponding to slack coefficients $\rho = (1.20; 1.13)$. This initial step reduces the required types of elements from 11 to 10. Figure 20b shows

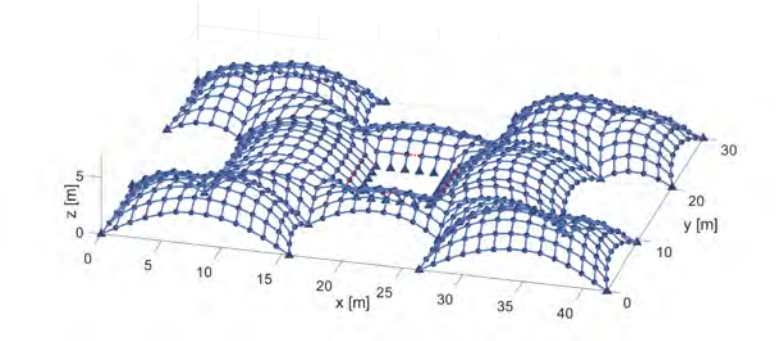

(a) $\rho = 1.06$

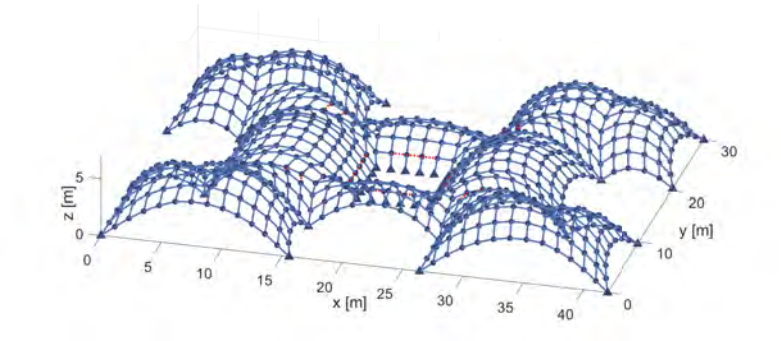

(b) $\rho = 1.12$

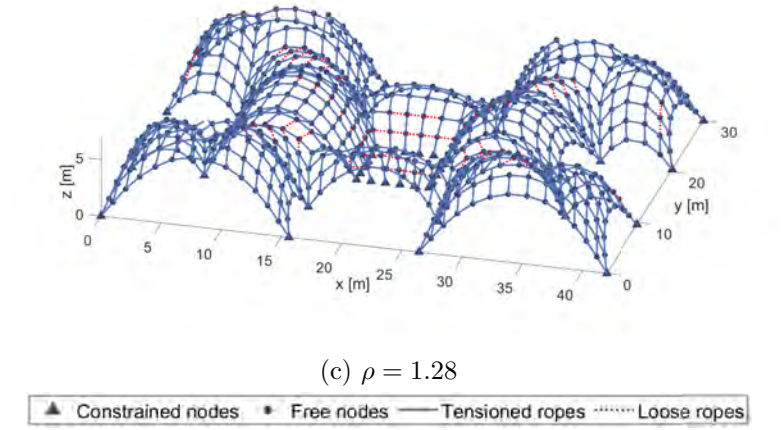

(c) $\rho = 1.28$

Figure 19: MRA application on symmetrical structure with a non-canonical geometric plan and opening in the center, for different slack coefficients: (a) $\rho = 1.06$, (b) $\rho = 1.12$, (c) $\rho = 1.28$.

the next step, which utilizes MO-MRA with three distinct target lengths, $L_{rope} = (1.44m; 1.35m; 1.30m)$, corresponding to $\rho = (1.20; 1.13; 1.08)$. As a result, a geometry is produced that can be constructed using only 5 different types of pieces, further reducing the required element typologies from 10 to 5. Finally, the RN-MRA is applied to the system in Figure 20b, taking into consideration that the loose ropes are only slightly shorter than the target lengths. This results in the geometry depicted in Figure 20c, which can be constructed using only 3 types of structural elements.

The changes in the distribution of element lengths for the distinct case studies in Figures 19 and 20 are depicted in Figures 21, 22, and 23. In particular, in Figure 21, the histograms illustrate the distribution of lengths after the application of the basic MRA. In addition, the reduction in element typologies resulting from the application of MO-MRA is evident in the distributions depicted in Figure 22. Finally, in Figure 21, the lengths distribution for the final configuration obtained through the complete i-MRA application is presented.

The third example highlights the significant benefits of using i-MRA on complex-shaped structures by simplifying the construction process management. By adopting this approach, the number of structural element classes that need to be managed on the construction site can be reduced from a maximum of 11 different types of components to just 3. Minor adjustments are made to the structural shape obtained with the basic MRA to achieve this reduction. The final geometry of the structure exhibits regularity and consistency with shapes determined using only form-finding techniques. This is crucial as it allows the structure to avoid significant deviations from the

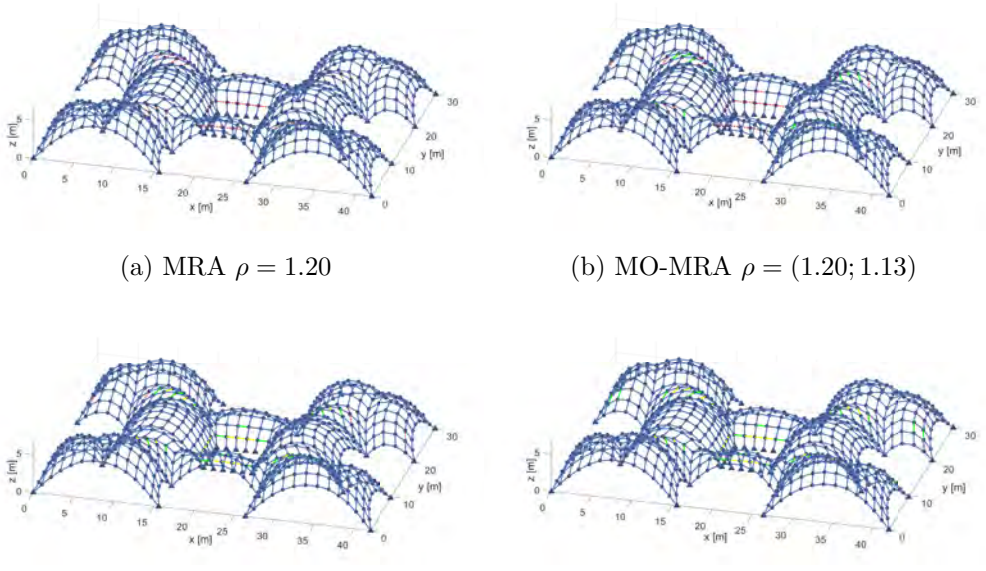

(a) MRA $\rho = 1.20$

(b) MO-MRA $\rho = (1.20; 1.13)$

(c) MO-MRA $\rho = (1.20; 1.13; 1.08)$

(d) Complete i-MRA $\rho = (1.20; 1.13; 1.08)$

Figure 20: i-MRA application on symmetrical structure with a non-canonical geometric plan and opening in the center.

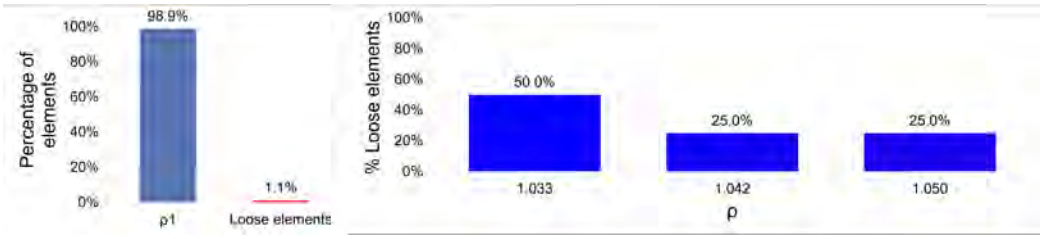

(a) $\rho = 1.06$

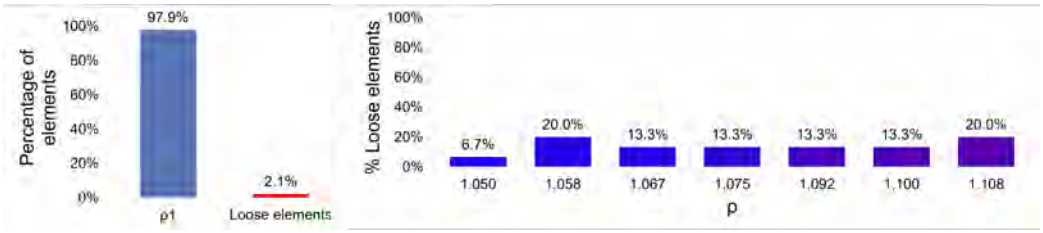

(b) $\rho = 1.12$

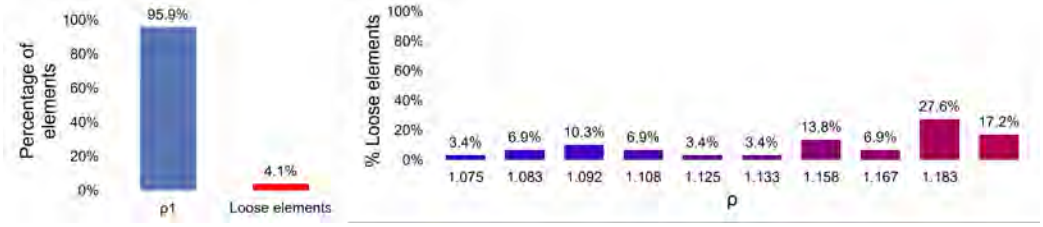

(c) $\rho = 1.20$

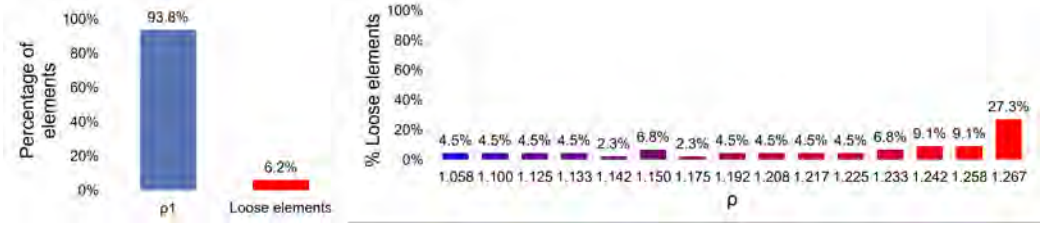

(d) $\rho = 1.28$

Figure 21: Application 3: Structural element lengths distribution applying the MRA.

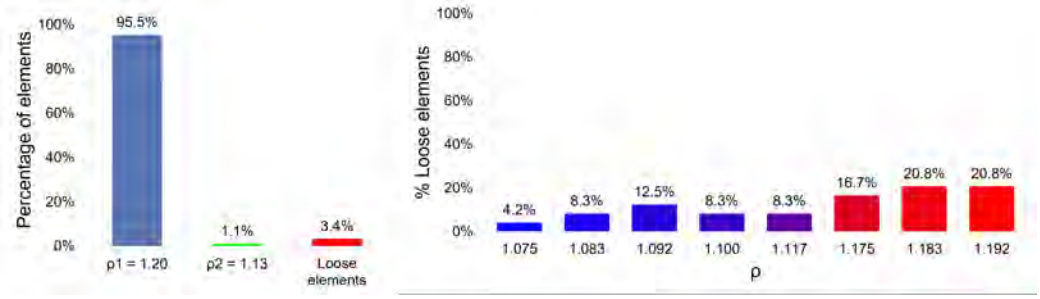

(a) MO-MRA $\rho = (1.20; 1.13)$

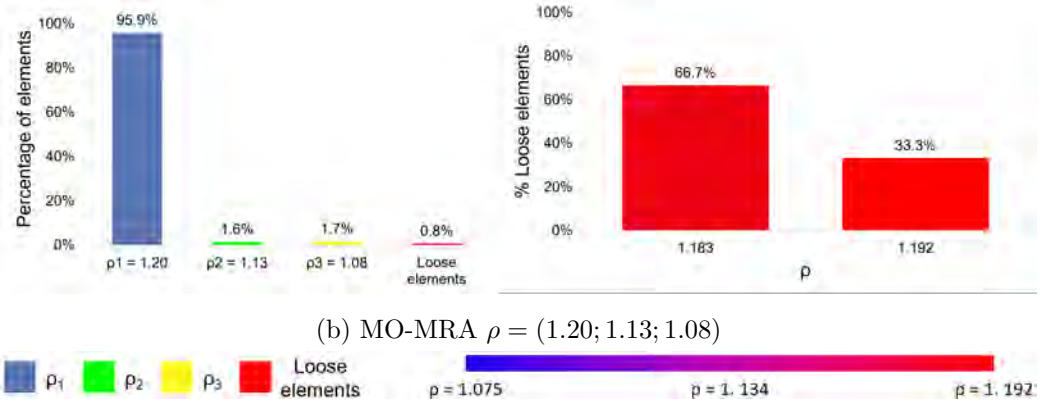

(b) MO-MRA $\rho = (1.20; 1.13; 1.08)$

Figure 22: Application 3: Structural element lengths distribution applying the MO-MRA.

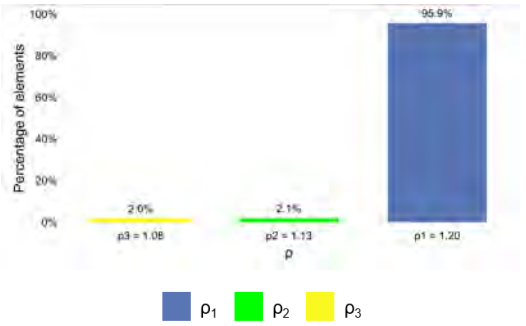

Figure 23: Application 3: Structural element lengths distribution applying the complete i-MRA.

funicular shape, which represents the optimal shape from a structural point of view.

The structural analyses presented in Figure 24 demonstrate that the geometries produced by basic MRA (on the left) and i-MRA (on the right) are very similar in terms of axial force (top), bending moment (middle), and Von Mises stress (bottom). This indicates that the deviations from the funicular shape obtained with i-MRA are minimal. In this case, the use of i-MRA results in a reduction of the structural components by five times, while the static behavior of the structure remains virtually unchanged.

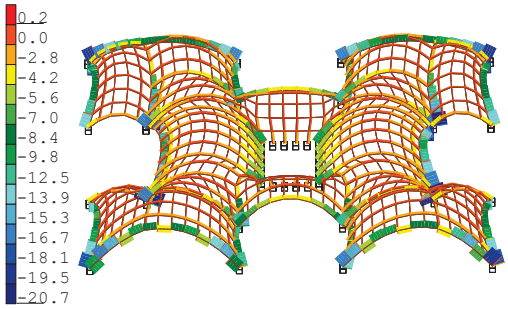

(a) MRA: $|N|_{max} = 20.7kN$

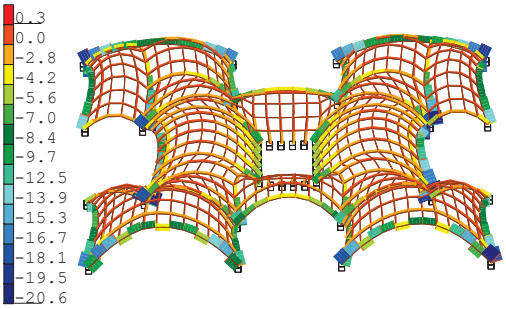

(b) i-MRA: $|N|_{max} = 20.6kN$

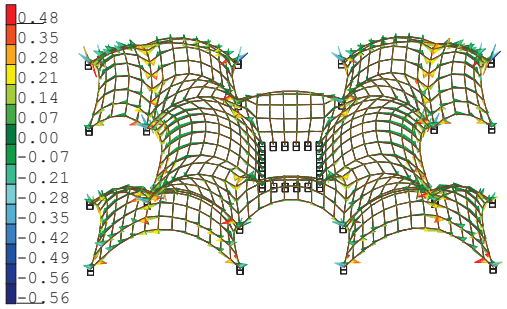

(c) MRA: $|M|_{max} = 0.56kNm$

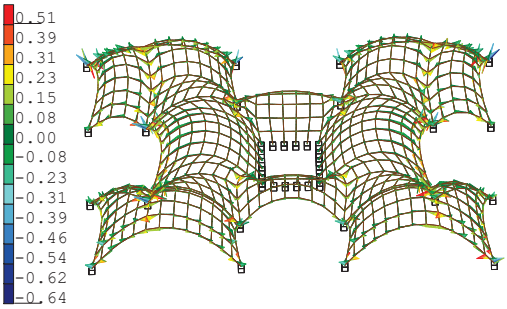

(d) i-MRA: $|M|_{max} = 0.64kNm$

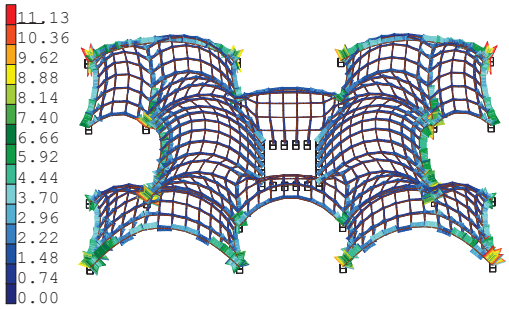

(e) MRA: $|\sigma^{VM}|_{max} = 11.13kPa$

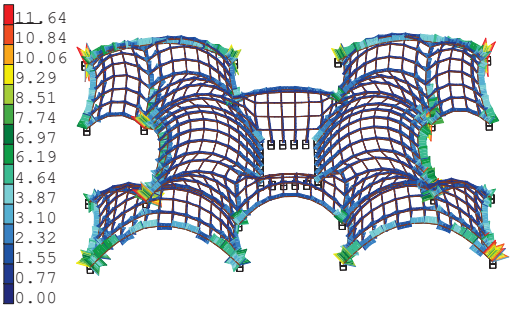

(f) i-MRA: $|\sigma^{VM}|_{max} = 11.64kPa$

Figure 24: Structural analysis performed on the structures obtained by applying basic MRA (left) and i-MRA (right) on the application example in Section 3.3. Comparison in terms of axial force [kN] (top), bending moment [kNm] (middle) and Von Mises stress [kPa] (bottom).

3.4. Application 4: Free-form geometry

The final application example aims to evaluate the effectiveness of the proposed approach in a highly general scenario. The method is applied by considering a base plan that is defined by a free-form curve, and the mesh is generated automatically using parametric design software. The analysis focuses on two types of meshes: the quadrangular mesh and the mesh formed by hexagonal and pentagonal elements. The meshes are generated with the goal of covering the reference surface as smoothly as possible. In this particular example, the basic mesh's constituent parts result in various sizes and shapes due to the surface's irregular layout. Consequently, this is the most complex application of MRA, as the proposed objective is to obtain equal structural elements from a geometry composed of different elements.

Both meshes presented in this section are made up of edges with an average length of about 1.50m. However, the elements that make up the quadrangular mesh in Figure 25*a* range in length from a minimum of about 0.80m to a maximum of about 2.30m, resulting in a considerable degree of variability in the starting elements.

In this example, each rope has its unique slack coefficient since the definition of the slack coefficient ρ is based on the initial distance between nodes (Equation 23) and takes into account that this distance varies for each pair of connected nodes. This implies that the coefficient is depicted as a vector with a length equal to the total number of ropes. To offer a comprehensive measure, ρ_{avg} is defined as the average of all the slack coefficients within the vector. Therefore, the definition of ρ_{avg} is reported in the following expression:

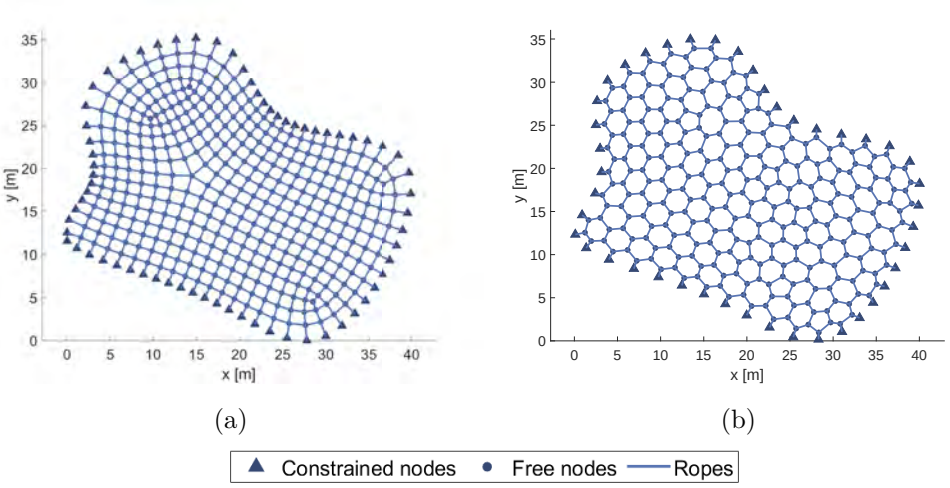

Figure 25: Different base mesh for free-form structure

$$\rho_{avg} = \frac{\sum_{i=1}^{n_{ropes}} (\rho_i)}{n_{ropes}} \tag{23}$$

The structural configuration obtained using the basic MRA with a $\rho_{avg} = 1.20$ for the quadrangular mesh case (Figure 25a) is shown in Figures 26a and 26c. In this case, red is used to indicate structural elements whose final length deviates from the target length of $L_{rope} = 1.78m$ (*loose ropes*). These elements constitute more than 13% of the 750 structural components that form the gridshell due to the basic geometry irregularities. As a result, more than 100 different structural elements are different from the target one in the actual structure. Although this may be manageable on the construction site, it can be challenging for generic and complex structural forms, making construction phase management more difficult than observed in previous examples.

The distribution of lengths for the structural elements in this case study is

depicted in Figure 27. The structure is characterized by 44 different element typologies, highlighting the variability of element types in this specific case study.

However, the structural configuration obtained by applying the i-MRA presented in this paper is shown in Figures 26*b* and 26*d*. The improvement achieved in this scenario is significant. The technique allowed for the calculation of a structural geometry that can be realized by employing only 6 structural component types of length $L_{rope} = [1.78; 1.58; 1.45; 1.35; 1.25; 1.15]m$. Figure 28 represents the distribution of structural elements among the 6 target lengths. This result is impressive and demonstrates how the techniques presented in Section 2 can substantially reduce construction complexity.

The results of the structural analyses presented in Figure 4 indicate that the changes in structural geometry achieved through i-MRA do not cause a significant increase in stresses. The structure calculated with i-MRA (right) experiences similar values of axial force and bending moment compared to the basic form-finding geometry (left). The application of i-MRA resulted in a decrease in the 6. Despite the geometric changes introduced, the imposed Von Mises stresses increased by less than 0.7 percent, which is a negligible increase. Moreover, the construction complexity of the work, as defined by the different types of structural elements used, was reduced by almost 10 times.

Finally, Figure 25*b* shows an interesting case of mesh composed of alternating hexagonal and pentagonal elements. This type of mesh is commonly used in geodesic dome design [45, 46, 47]. The advantage of this pattern lies in its ability to cover curved regular surfaces with geometrically regu-

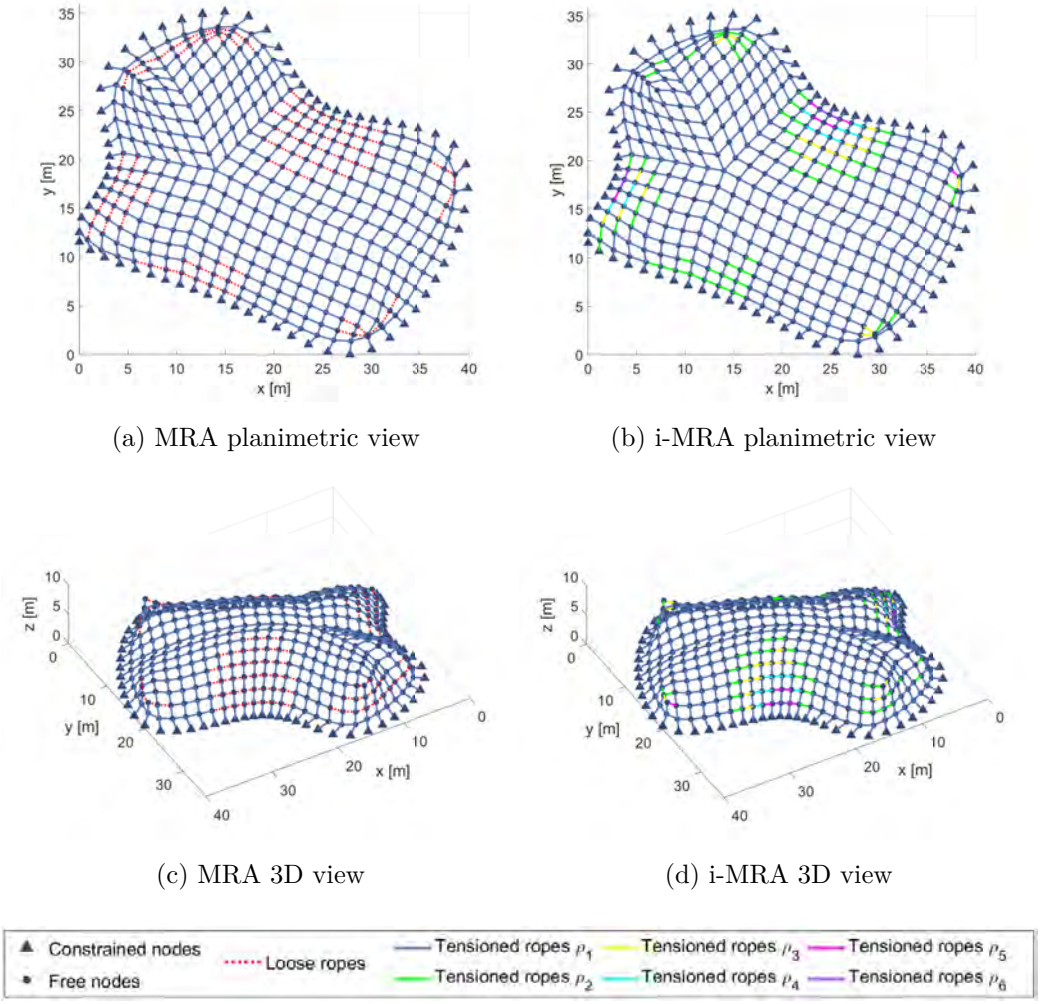

(a) MRA planimetric view

(b) i-MRA planimetric view

(c) MRA 3D view

(d) i-MRA 3D view

Figure 26: Comparison between MRA and i-MRA on a free-form structure with quadrangular mesh.

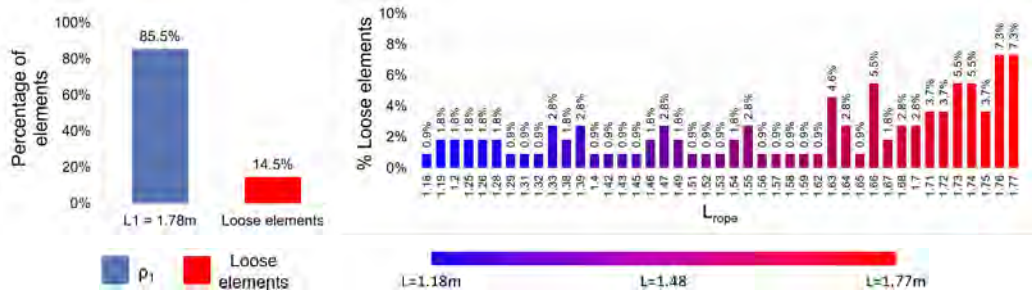

Figure 27: Application 4: Structural element lengths distribution applying the MRA.

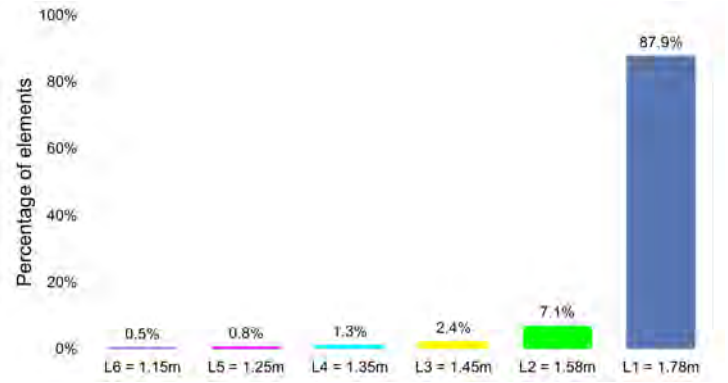

Figure 28: Application 4: Structural element lengths distribution applying the i-MRA.

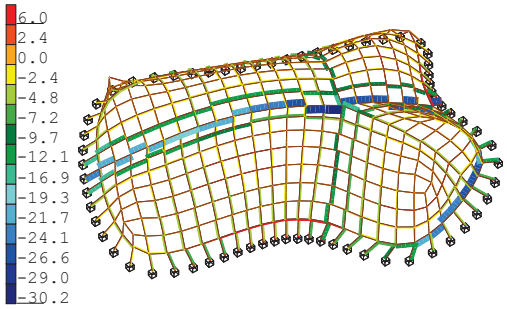

(a) MRA: $|N|_{max} = 6.0kN$

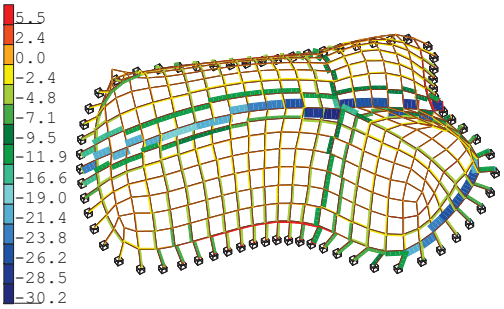

(b) i-MRA: $|N|_{max} = 5.5kN$

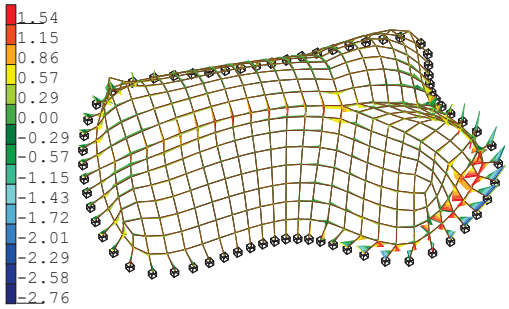

(c) MRA: $|M|_{max} = 2.76kNm$

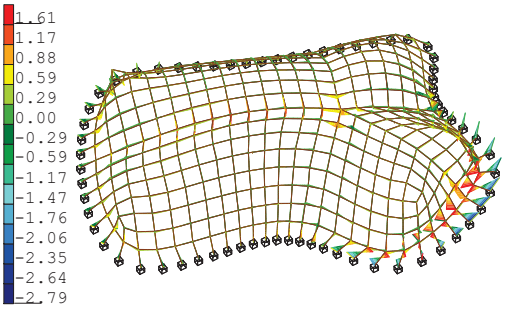

(d) i-MRA: $|M|_{max} = 2.79kNm$

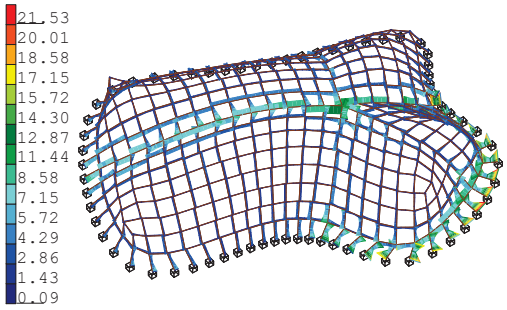

(e) MRA: $|\sigma^{VM}|_{max} = 21.53kPa$

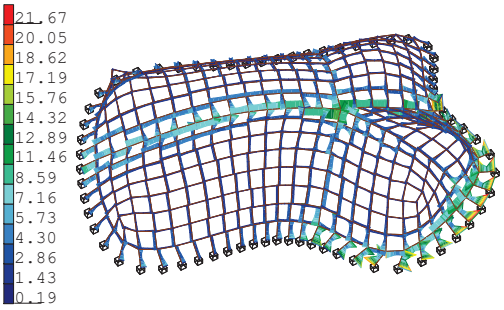

(f) i-MRA: $|\sigma^{VM}|_{max} = 21.67kPa$

Figure 29: Structural analysis performed on the structures obtained by applying basic MRA (left) and i-MRA (right) on the application example with quadrangular mesh in Section 3.4. Comparison in terms of axial force [kN] (top), bending moment [kNm] (middle) and Von Mises stress [kPa] (bottom).

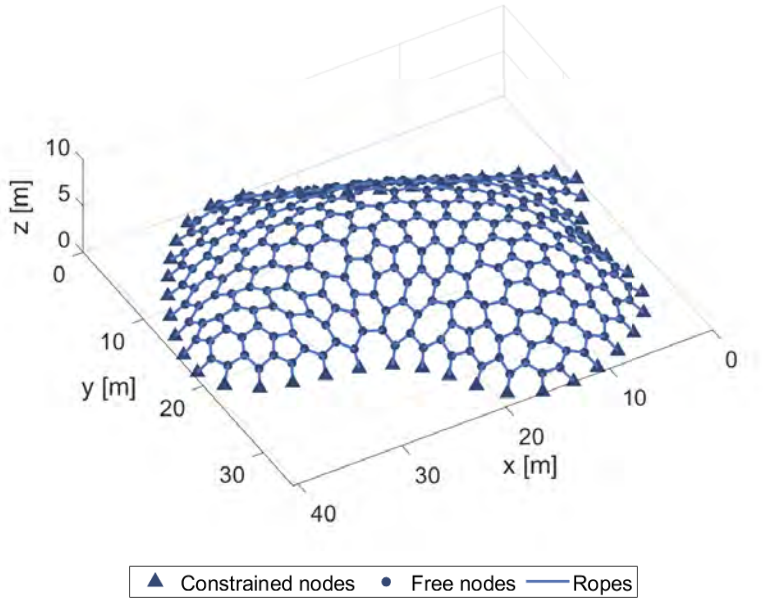

Figure 30: MRA application on a free-form structure with hexagonal mesh and $\rho = 1.10$.

lar planar elements. In fact, spherical domes are often designed using this pattern.

In the presented example, the benefit of adopting this particular mesh is related to the fact that each node is connected to a maximum of three adjacent nodes. As a result, each node is constrained by a maximum of three ropes, and the three degrees of freedom related to spatial translations are tied by three ropes. This less restrictive system can evolve towards an equilibrium configuration in which all the ropes composing the entire network are tense. The direct outcome is that the geometry obtained by applying the basic MRA is very shallow and consists of a single type of structural element, as shown in Figure 30.

4. Conclusions

This paper presents a form-finding method that is specifically designed for gridshell structures. The method builds upon the Multi-body Rope Approach (MRA) developed by [29]. Once a load condition is defined, the basic MRA allows for the definition of the structural geometry that is characterized by the smaller eccentricity of applied compression forces. This helps to reduce bending moments and applied stress. The structure is modeled as a network of masses that are connected by loose ropes, and the solution of the dynamics of the system, subject to a specific load condition, allows the definition of a final equilibrium configuration that represents the structural geometry with the lowest bending moment.

To further minimize the complexity of structural construction management and reduce computational effort, two improvement techniques are proposed for the basic MRA. The first technique involves defining groups of structural elements with identical lengths, which helps to minimize the types of structural elements required for constructing the calculated structures. The second technique involves applying a repulsive force field to the dynamic model, which allows for tiny adjustments of the geometry to limit the number of structural components that do not fit into the previously established groups. The combination of these two techniques is referred to as i-MRA.

The effectiveness of the proposed method was tested in four application examples of increasing complexity. The results showed that the i-MRA method leads to a significant reduction in the number of structural components required, especially as the geometric complexity of the structure increases.

The results of the structural analyses indicate that i-MRA induced changes on funicular structures calculated with basic MRA do not have significant impacts on their static behaviour. The increases observed in terms of internal actions and stress were less than 1 % for almost all of the cases studied. Consequently, reducing the number of components analyzed has no adverse consequences from a structural perspective. However, it has important implications such as reducing production costs, encouraging mass production, and lowering expenses related to construction management.

The studied examples also demonstrated that the base mesh has no discernible influence on the law connecting the slack coefficient to the structural height, which remains consistent in its qualitative trend.

However, the research also revealed that the initial mesh has a significant impact on the final structural geometry. Thus, the selection of the basic mesh type is crucial. The research presented in this paper provides a foundation for further investigations on the subject, with potential future developments including an analysis of how the introduced methods may affect structural performance. Specifically, future research could investigate how the introduced geometric variations may impact the instability of the analyzed structures. Such an analysis could prove beneficial to both science and design practice.

Moreover, the proposed approach could be introduced into a structural optimization procedure, which could identify the optimal parameters for generating the most effective structural shape while minimizing the costs associated with the projected structure. Finally, exploring and optimizing the optimal shapes for the panels and nodes that constitute the structure of the

gridshell could also represent an interesting research topic.

Indeed, while the methods presented in this paper can be helpful in achieving more efficient and cost-effective structures, the role of the designer remains critical. The designer's knowledge and experience are essential in making informed decisions and balancing the trade-offs between structural performance, aesthetic appeal, and cost-effectiveness. The proposed methods should be seen as tools that can support the designer in the decision-making process, rather than a substitute for their expertise. It is through the collaboration between the designer and the computational tools that the most optimal and effective design solutions can be achieved.

5. Acknowledgments

The authors acknowledge A. Brentegani for her contribution to the implementation of the Matlab codes for the method presented in this paper.

References

[1] J. N. Richardson, S. Adriaenssens, R. Filomeno Coelho, P. Bouillard, Coupled form-finding and grid optimization approach for single layer grid shells, Engineering Structures 52 (2013) 230–239. doi:https://doi.org/10.1016/j.engstruct.2013.02.017.

[2] J. Chilton, C.-C. Chuang, Rooted in nature: aesthetics, geometry and structure in the shells of heinz isler, Nexus Network Journal 19 (3) (2017) 763–785. doi:https://doi.org/10.1007/s00004-017-0357-5.

[3] X. Tellier, Bundling elastic gridshells with alignable nets. part ii: Form-finding, Automation in Construction 141 (2022) 104292. doi:https://doi.org/10.1016/j.autcon.2022.104292.

URL https://www.sciencedirect.com/science/article/pii/S0926580522001650

[4] V. Tomei, E. Grande, M. Imbimbo, Design optimization of gridshells equipped with pre-tensioned rods, Journal of Building Engineering 52 (2022) 104407. doi:https://doi.org/10.1016/j.jobe.2022.104407.
URL https://www.sciencedirect.com/science/article/pii/S235271022200420X

[5] F. Otto, J. Hennicke, K. Matsushita, Il10 gitterschalen, Institut für leichte Flächentragwerke (IL)ISBN: 378282010X (1974).

[6] E. Happold, Philosophy of design with particular respect to buildings, London: E & FN Spon, 1997, ISBN: 9780429080012.

[7] B. Addis, D. Walker, Happold: The confidence to build, Taylor & Francis, 2005, ISBN: 9780203976487. doi:https://doi.org/10.4324/9780203976487.

[8] I. Liddell, Frei otto and the development of gridshells, Case Studies in Structural Engineering 4 (2015) 39–49. doi:https://doi.org/10.1016/j.csse.2015.08.001.
URL https://www.sciencedirect.com/science/article/pii/S2214399815300011

[9] W. Pan, M. Turrin, C. Louter, S. Sariyildiz, Y. Sun, Integrating multi-functional space and long-span structure in the early design stage of indoor sports arenas by using parametric modelling and multi-objective optimization, Journal of Building Engineering 22 (2019) 464–485. doi:https://doi.org/10.1016/j.jobe.2019.01.006.
URL https://www.sciencedirect.com/science/article/pii/S2352710218304467

[10] W. Sobek, L. Blandini, The mansueto library–notes on a glazed steel grid shell from design to construction, in: Challenging Glass Conference Proceedings, Vol. 2, 2010, pp. 179–186. doi:https://doi.org/10.7480/cgc.2.2316.

[11] K. Fritzsche, W. van der Sluis, E. Smits, J. Bakker, Capital c, geometric optimization of a free-form steel gridshell towards planar quadrilateral glass units, in: Challenging Glass Conference Proceedings, Vol. 7, 2020. doi:https://doi.org/10.7480/cgc.7.4493.

[12] C. Zhao, J. Ma, S. Du, Y. Gu, Y. Zhou, Mechanical properties of a novel joint of a single-layer aluminum-alloy combined lattice-shell structure, Materiali in tehnologije 53 (2019) 811–819. doi:https://doi.org/10.1007/s12205-021-0239-y.

[13] E. Happold, L. WI, Timber lattice roof for the mannheim bundesgartenschau, The structural engineer 53 (1975) 99–135.
URL https://docplayer.net/126675850-Timber-lattice-roof-for-the-mannheim-bundesgartenschau.html

[14] R. Harris, Design of timber gridded shell structures, Proceedings of the Institution of Civil Engineers - Structures and Buildings 164 (2) (2011) 105–116. doi:10.1680/stbu.9.00088.

[15] M. Collins, T. Cosgrove, A review of the state of the art of timber gridshell design and construction, in: Civil Engineering Research in Ireland CERI 2016 Conference Proceeding, Civil Engineering Research Association of Ireland CERAI, 2016.
URL https://hdl.handle.net/10344/5192

[16] J. Chilton, G. Tang, Timber gridshells: architecture, structure and craft, Routledge, 2016, ISBN: 9781138775305. doi:https://doi.org/10.4324/9781315773872.

[17] C. Douthe, J. Caron, O. Baverel, Gridshell structures in glass fibre reinforced polymers, Construction and Building Materials 24 (9) (2010) 1580–1589. doi:https://doi.org/10.1016/j.conbuildmat.2010.02.037.
URL https://www.sciencedirect.com/science/article/pii/S0950061810000802

[18] F. T. Olivier Baverel, Jean-François Caron, L. D. Peloux, Gridshells in composite materials: Construction of a 300 m2 forum for the solidays' festival in

paris, Structural Engineering International 22 (3) (2012) 408–414. doi:10.2749/101686612X13363869853572.

[19] B. D'Amico, A. Kermani, H. Zhang, A. Pugnale, S. Colabella, S. Pone, Timber gridshells: Numerical simulation, design and construction of a full scale structure, Structures 3 (2015) 227–235. doi:https://doi.org/10.1016/j.istruc.2015.05.002.
URL https://www.sciencedirect.com/science/article/pii/S2352012415000557

[20] M. Bagneris, R. Motro, B. Maurin, N. Pauli, Structural morphology issues in conceptual design of double curved systems, International Journal of Space Structures 23 (2) (2008) 79–87. doi:10.1260/026635108785260560.

[21] E. L. Hernández, O. Baverel, C. Gengnagel, On the design and construction of elastic gridshells with irregular meshes, International Journal of Space Structures 28 (3-4) (2013) 161–174. doi:10.1260/0266-3511.28.3-4.161.

[22] S. H. Dyvik, B. Manum, A. Rønnquist, Gridshells in recent research—a systematic mapping study, Applied Sciences 11 (24) (2021). doi:10.3390/app112411731.
URL https://www.mdpi.com/2076-3417/11/24/11731

[23] L. Gründig, E. Moncrieff, P. Singer, D. Ströbel, A history of the principal developments and applications of the force density method in germany 1970–1999, in: Proceedings of IASS-IACM 2000 Fourth International Colloquium on Computation of Shell & Spatial Structures, Chania-Crete, Greece, 2000.
URL https://www.technet-gmbh.com/fileadmin/user_upload/technet/Publikationen/Easy/Density2.pdf

[24] R. Mesnil, C. Douthe, O. Baverel, T. Gobin, Form finding of nexorades using the translations method, Automation in Construction 95 (2018) 142–154. doi:https://doi.org/10.1016/j.autcon.2018.08.010.
URL https://www.sciencedirect.com/science/article/pii/S092658051830147X

[25] H.-J. Schek, The force density method for form finding and computation of general networks, Computer Methods in Applied Mechanics and Engineering 3 (1) (1974) 115–134. doi:https://doi.org/10.1016/0045-7825(74)90045-0.
URL https://www.sciencedirect.com/science/article/pii/0045782574900450

[26] J. R. H. OTTER, A. C. CASSELL, R. E. a. HOBBS, Dynamic relaxation, Proceedings of the Institution of Civil Engineers 35 (4) (1966) 633–656. doi:10.1680/iicep.1966.8604.

[27] P. Block, J. Ochsendorf, Thrust network analysis: A new methodology for three-dimensional equilibrium, Journal of the International Association for Shell and Spatial Structures 48 (3) (2007) 167–173.
URL https://www.ingentaconnect.com/content/iass/jiass/2007/00000048/00000003/art00011

[28] A. Kilian, J. Ochsendorf, Particle-spring systems for structural form finding, Journal of the International Association for Shell and Spatial Structures 46 (2) (2005) 77–84.
URL https://www.ingentaconnect.com/content/iass/jiass/2005/00000046/00000002/art00003

[29] A. Manuello, Multi-body rope approach for grid shells: Form-finding and imperfection sensitivity, Engineering Structures 221 (2020) 111029. doi:https://doi.org/10.1016/j.engstruct.2020.111029.
URL https://www.sciencedirect.com/science/article/pii/S0141029620309895

[30] I. M. Rian, M. Sassone, S. Asayama, From fractal geometry to architecture: Designing a grid-shell-like structure using the takagi–landsberg surface, Computer-Aided Design 98 (2018) 40–53. doi:https://doi.org/10.1016/j.cad.2018.01.004.
URL https://www.sciencedirect.com/science/article/pii/S0010448518300423

[31] Z. Zhao, D. Yu, T. Zhang, N. Zhang, H. Liu, B. Liang, L. Xian, Efficient form-finding algorithm for freeform grid structures based on inverse hanging method, Journal of Building Engineering 46 (2022) 103746. doi:https://doi.org/10.1016/j.jobe.2021.103746.
URL https://www.sciencedirect.com/science/article/pii/S2352710221016041

[32] W. Huang, C. Wu, J. Hu, W. Gao, Weaving structure: A bending-active gridshell for freeform fabrication, Automation in Construction 136 (2022) 104184. doi:https://doi.org/10.1016/j.autcon.2022.104184.
URL https://www.sciencedirect.com/science/article/pii/S0926580522000577

[33] K. Yamamoto, T. Ogawa, M. Fujimoto, C. Lazaro, T. Takeuchi, S.-D. Xue, P.-S. Chen, S. Kato, State-of-the-art for optimization of forms and strength for reticulated shells, in: International Association for Shell and Spatial Structures 2012: From Spatial Structures to Space Structures, 2012.

[34] S. Adriaenssens, P. Block, D. Veenendaal, C. Williams, Shell structures for architecture: form finding and optimization, Routledge, 2014, ISBN: 9780415840606. doi:https://doi.org/10.4324/9781315849270.

[35] L. Bouhaya, O. Baverel, J.-F. Caron, Optimization of gridshell bar orientation using a simplified genetic approach, Structural and Multidisciplinary Optimization 50 (2014) 839–848. doi:https://doi.org/10.1007/s00158-014-1088-9.

[36] C. Douthe, R. Mesnil, H. Orts, O. Baverel, Isoradial meshes: Covering elastic gridshells with planar facets, Automation in Construction 83 (2017) 222–236. doi:https://doi.org/10.1016/j.autcon.2017.08.015.
URL https://www.sciencedirect.com/science/article/pii/S0926580517307367

[37] N. Montagne, C. Douthe, X. Tellier, C. Fivet, O. Baverel, Discrete voss surfaces: Designing geodesic gridshells with planar cladding panels, Automation in Construc-

tion 140 (2022) 104200. doi:https://doi.org/10.1016/j.autcon.2022.104200.
URL https://www.sciencedirect.com/science/article/pii/S0926580522000735

[38] H. Seifi, A. Rezaee Javan, S. Xu, Y. Zhao, Y. M. Xie, Design optimization and additive manufacturing of nodes in gridshell structures, Engineering Structures 160 (2018) 161–170. doi:https://doi.org/10.1016/j.engstruct.2018.01.036.
URL https://www.sciencedirect.com/science/article/pii/S0141029617320564

[39] I. M. de Oliveira, R. M. de Oliveira Pauletti, L. C. Meneghetti, Connection system for gridshell structures using parametric modeling and digital fabrication, Automation in Construction 109 (2020) 102996. doi:https://doi.org/10.1016/j.autcon.2019.102996.
URL https://www.sciencedirect.com/science/article/pii/S0926580519306612

[40] A. M. Bertetto, F. Riberi, Form-finding of pierced vaults and digital fabrication of scaled prototype, Curved and Layered Structures 8 (1) (2021) 210–224 [cited 2023-11-08]. doi:doi:10.1515/cls-2021-0020.
URL https://doi.org/10.1515/cls-2021-0020

[41] A. Manuello Bertetto, J. Melchiorre, L. Sardone, G. Marano, et al., Multi-body rope approach for the form-finding of shape optimized grid shell structures, in: Pursuing the Infinite Potential of Computational Mechanics, International Centre for Numerical Methods in Engineering, CIMNE, 2022. doi:10.23967/wccm-apcom.2022.075.

[42] SOFiSTiK, Text Editor 2023, Flataustr. 14, 90411 Nuremberg, 2022.
URL https://www.https://www.sofistik.com(lastvisited:8November2023)

[43] J. Melchiorre, S. Soutiropoulos, A. Manuello Bertetto, G. C. Marano, F. Marmo, Grid-shell multi-step structural optimization with improved multi-body rope approach and multi-objective genetic algorithm, in: S. Gabriele, A. Manuello Bertetto,

F. Marmo, A. Micheletti (Eds.), Shell and Spatial Structures, Springer Nature Switzerland, Cham, 2024, pp. 62–72. doi:https://doi.org/10.1007/978-3-031-44328-2_7.

[44] MATLAB, version (R2022b) access (8 November 2023), The MathWorks Inc., Natick, Massachusetts, 2022.
URL https://www.mathworks.com/products/matlab.html

[45] T. Tarnai, Geodesic domes and fullerenes, Philosophical Transactions of the Royal Society of London. Series A: Physical and Engineering Sciences 343 (1667) (1993) 145–154. doi:https://doi.org/10.1098/rsta.1993.0048.

[46] G. Pavlov, Geodesic domes bounded by symmetrical mainly hexagonal elements, International Journal of Space Structures 9 (2) (1994) 53–66. doi:10.1177/026635119400900201.

[47] H. Miura, M. Kimoto, A comparison of grid quality of optimized spherical hexagonal–pentagonal geodesic grids, Monthly Weather Review 133 (10) (2005) 2817 – 2833. doi:https://doi.org/10.1175/MWR2991.1.
URL https://journals.ametsoc.org/view/journals/mwre/133/10/mwr2991.1.xml